

# Natural Associativity without the Pentagon Condition

**William P. Joyce**

Department of Physics and Astronomy, University of Canterbury, Private Bag 4800, Christchurch, New Zealand.

email:w.joyce@phys.canterbury.ac.nz

**Abstract.** A premonoidal category is equipped only with a bifunctor and a natural isomorphism for associativity. We introduce a (deformation) natural automorphism,  $\mathfrak{q}$ , representing the deviation from the Pentagon condition. We uncover a binary tree representation for all diagrams involving  $\mathfrak{a}$  and  $\mathfrak{q}$  and provide a link to permutations and linear orderings. This leads to other notions of premonoidality. We define these notions and prove coherence results for each.

PACS number: 02.10.Ws, 02.20.Qs, 02.20.Fh, 02.20.Df, 03.65.Fd, 31.15.Hz

## 1. Introduction

An initial motivation for this paper is to address a simple short-coming of monoidal categories. Namely the construction of a purely fermionic statistics. Furthermore, to generalise statistical structures in a physically meaningful way. In other words a commutativity constraint given by  $a \otimes b = -b \otimes a$ . According to the Hexagon diagram this requires associativity to be given by  $(a \otimes b) \otimes c = -a \otimes (b \otimes c)$ . The Pentagon diagram rules this possibility out. This paper describes the structure required for such a choice and its natural extensions. We begin with a natural isomorphism for associativity onto which we progressively add other structures. This basic structure is called premonoidal since the Pentagon diagram does not hold and the notion of identity is omitted.

The notion of coherence also changes. It is not possible to construct a template premonoidal structure which can be shown to be related by a premonoidal functor equivalence to every other premonoidal structure. Instead we only ask for a groupoid whose diagrams somehow encode the coherent diagrams of the premonoidal structure; and a functor for interpreting these diagrams as diagrams in the category of interest. Coherence asserts that all diagrams arising in this way commute. This potentially leaves many diagrams in the category of interest that do not commute. Furthermore, the interpreting functor is not necessarily faithful. The advantages of this approach are manifold. The coherent diagrams are represented by rooted planar binary trees with levels and formal primitive operations on these trees. There is a close connection with permutations and linear orderings. This avoids Catalan numbers and, in my view, simplifies the combinatorics. Moreover, this provides a link between associativity and transpositions.

Premonoidal category structure has an important role to play in the exploration of non-associative particle statistics in quantum theories, see Joyce [1, 2, 3, 4, 5]. Recently an origin has been suggested for quark state confinement utilising a premonoidal statistic for  $SU(3)$  colour, see Joyce [6]. Related to this is the issue of coupling (of quantum states) which has ambiguity. For example, in the expression  $(a \otimes b) \otimes (c \otimes d)$  there is an ambiguity concerning whether  $a$  and  $b$  are coupled to form  $a \otimes b$ , before or after coupling  $c$  and  $d$  to form  $c \otimes d$ . In a premonoidal category the distinction is taken into account. This removes all freedom in the projection of diagrams in the Racah-Wigner calculus, see Joyce [7]. The coherence groupoid represents the coupling of the category. It is important to note that the premonoidal category may in fact admit a monoidal structure. Nevertheless, the structure of interest, representing non-associative particle statistics or an unambiguous coupling scheme, is premonoidal. It may well be that there exist very few premonoidal categories that do not admit a monoidal structure.

Monoidal categories were explicitly defined by Benabou [8] and Mac Lane [9, 10]. The monoidal category structure is found in many areas of physics. In quantum groups and knot theory [11], the Racah-Wigner calculus [12, 13] and Feynman diagrams. The notion of coherence has its origin in Mac Lane [9] with the modifications of Kelly [14] and in Stasheff [15]. The original work studied natural isomorphisms for associativity,

a symmetric commutativity and identity. These were extended to cover distributivity by Kelly [16] and Laplaza [17]. The non-symmetric or braided commutativity was studied in Joyal and Street [18]. This paper re-examines natural associativity but without the Pentagon condition. An alternative and entirely different account by Yanofsky [19] was brought to my attention by Prof. Ross Street during the final stages of preparing this paper. The Yanofsky approach is based on higher dimensional category theory. In contrast this approach is based on binary trees and a natural automorphism,  $\mathfrak{q}$ , accounting for the non-commutativity of the Pentagon diagram. Further to this structure we may incorporate to  $\mathfrak{q}$ -Square diagrams giving a pseudomonoidal structure. One may think of the automorphism  $\mathfrak{q}$  as a deformation of the Pentagon diagram. The power of this approach is realised by the binary tree representation of coherent diagrams. The natural automorphism  $\mathfrak{q}$  has the simple interpretation of interchanging the level of internal nodes. This insight suggests the obvious extension to interchange of terminal nodes called  $\mathfrak{q}$ -pseudomonoidal.

The incorporation of the notion of identity has proven to be a delicate balance between pseudomonoidal and  $\mathfrak{q}$ -pseudomonoidal structures. This intermediate structure is called  $\mathfrak{q}$ -braided pseudomonoidal. One can always account for identities by imposing the Triangle diagram. This ultimately conflicts with the motivation behind this paper. Although the  $\mathfrak{q}$ -braided pseudomonoidal structure carries a true  $\mathfrak{q}$ -identity structure, coherence results from a finite number of diagrams only in the presence of a symmetric commutativity.

In section two we define the notion of binary tree required for what follows. Also we define the notion of coherence for premonoidal structures. Section three defines a premonoidal and pseudomonoidal categories, introduces  $\mathfrak{q}$ , the coherence groupoid and proves coherence. These two sections illustrate the methodology underlying this paper. In section four we spell out the link to permutations and linear orderings and briefly discuss polytopes. Section five extends the notion of a pseudomonoidal category to the stronger  $\mathfrak{q}$ -pseudomonoidal category. This requires extra diagrams. Namely the Dodecagon diagram and two Quaddecagon diagrams. The coherence theorem proved in this section is the major proof of this paper. Section six defines  $\mathfrak{q}$ -braided pseudomonoidal categories which relaxes the conditions of section five. Only the Decagon diagram and  $\mathfrak{q}$ -Pentagon diagram are retained. This section uncovers a braid structure for  $\mathfrak{q}$  where it is revealed that the Dodecagon diagram is a Yang-Baxter condition. We call  $\mathfrak{q}$  a  $\mathfrak{q}$ -braid because it satisfies a braid coherence result but differs from a usual braid in that no objects are interchanged.

In section seven we begin the quest for a  $\mathfrak{q}$ -monoidal structure by adding identities to pseudomonoidal structures. The result is given the prefix restricted. They are monoidal whenever the identity object indexes the natural isomorphisms. Section eight incorporates a symmetric commutativity natural isomorphism into a  $\mathfrak{q}$ -pseudomonoidal category. This requires  $\mathfrak{q}$  to be symmetric, the usual Hexagon diagram, a square diagram and two decagon diagrams. The symmetric pseudomonoidal category requires an additional two square diagrams. In section nine we give what rightly deserves to be

called a symmetric  $\mathfrak{q}$ -monoidal category. This requires the large and small  $\mathfrak{q}$ -Triangle diagrams. Section ten is a summary of the premonoidal structures of this paper.

## 2. Coherence

This section is an outline of the notion of, and the approach taken to coherence in this paper. Also much of the notation used in the following sections is established here. For each premonoidal type structure presented we need a category that formally encodes what diagrams should commute. All such categories in this paper will be some groupoid of rooted planar binary trees for which each node (of each tree) is assigned a level. We begin by making this notion of planar binary tree precise. Note that we reserve the term vertex for diagrams. Instead we use the term node.

A prerigid binary tree is a quadruple  $B = (V, E, l, s)$  consisting of a set of nodes  $V$ , a set of edges  $E \subset V \times V$ , a level function  $l : V \rightarrow \mathbb{N} \cup \{0\}$  and a hand function  $s : \{v \in V : l(v) \neq 0\} \rightarrow \{l, r\}$  with the properties:  $(V, E)$  is a rooted binary tree; the tree grows upward; there are no levels skipped; and all but the empty tree have a node at level 0. The unique node at level 0 is the only valency two node and is called the root. The nodes of valency one are called leaves. The nodes of valency three are called branches (shorthand for branch point). The branch nodes and the root node are called internal nodes while the leaves are terminal nodes. The terminates (or children) for an internal node are the two unique higher level nodes to which it is attached. We define the height of  $B$  to be  $\overline{B} = \max l(V)$ . The height is the level of at least one leaf. Note that  $\log_2 |V| \leq \overline{B} \leq |V|$ . The hand function  $s$  assigns a left hand ( $l$ ) or right hand ( $r$ ) side to each terminate at any given internal node. Two prerigid binary trees are isomorphic if there is a bijective function between their respective node sets preserving edges and the level and hand maps.

A rigid binary tree is an isomorphism class of prerigid binary trees. Thus every rigid binary tree is independent of an particular set of nodes. The name rigid is justified because there is absolutely no topological freedom in how the binary tree can be drawn in a plane provided we stipulate that edges do not cross. Moreover, this allows us to assign a relative position to the leaves. We number leaf positions in order from left to right (tracing around the top boundary of the tree). A typical example of a rigid binary tree is given in figure 1. The nodes occur where lines join. We have labelled the levels and

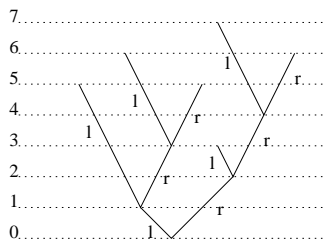


Figure 1. An example of a typical rigid binary tree.

hands. There is no need to do this and in what follows we dispense with labelling rigid binary trees except when emphasis is required.

Let  $\mathcal{C}$  be a category with some premonoidal type structure. There are many interesting and useful choices of this structure. For now we simply accept that  $\mathcal{C}$  carries some such structure. We construct a free groupoid  $\mathcal{B}$  over some class of rigid binary trees, together with a length function  $|\_|\_ : \mathcal{B} \rightarrow \mathbb{N} \cup \{0\}$  such that

$$\mathcal{B} = \prod_{n=0}^{\infty} \mathcal{B}_n \tag{1}$$

where  $\mathcal{B}_n$  is the free groupoid such that  $|B| = n$  for all  $B \in \mathcal{B}_n$ . The groupoid  $\mathcal{B}$  encodes the coherent diagrams for the structure of  $\mathcal{C}$ . These groupoids are not assumed to have a monoidal structure in any sense. The objects are given by the particular class of rigid binary trees. The arrows will be generated from a collection of invertible primitive arrows corresponding to formal binary tree operations. We call  $\mathcal{B}$  the coherence groupoid for the structure on  $\mathcal{C}$ .

All the diagrams we can construct in the category  $\mathcal{B}$  will underlie diagrams in  $\mathcal{C}$  that commute. A general diagram in  $\mathcal{B}$  is any closed finite directed graph. The boundary encircling each enclosed region defines a polygonal directed graph. Every general diagram is equivalent to the collection of polygonal directed graphs defined by its regions. We use the word diagram in this paper to mean a polygonal directed graph. Equivalently, a diagram is a functor into  $\mathcal{B}$  from the category of two objects and two parallel arrows. The collection of all diagrams for  $\mathcal{B}$  is denoted  $\mathcal{D}(\mathcal{B})$ . Moreover,

$$\mathcal{D}(\mathcal{B}) = \prod_{n=0}^{\infty} \mathcal{D}(\mathcal{B}_n) \tag{2}$$

The relationship between  $\mathcal{D}(\mathcal{B})$  and the (expected) coherent diagrams in  $\mathcal{C}$  is functorial. The functor of interest is the functor

$$\mathbf{can} : \mathcal{B} \rightarrow \prod_{n=0}^{\infty} [\mathcal{C}^n, \mathcal{C}] , \tag{3}$$

called the canonical functor, where  $\mathbf{can}(B) \in [\mathcal{C}^{|B|}, \mathcal{C}]$ . Although the explicit details depend on the particular structure of interest, we still give an outline of its construction here. It is defined inductively according to the length of a binary tree  $B \in \mathcal{B}$ . The length of the binary tree  $n$  determines that  $\mathbf{can}(B)$  is an object in  $[\mathcal{C}^n, \mathcal{C}]$ . We call the branches of  $B$  whose levels attain the greatest level among all branch levels couples for  $B$ . We will be interested in classes of rigid trees where every branch has a distinct level and hence every tree has a unique couple. Locate the position of the left hand most couple in  $B$ . The terminates are leaves and have positions  $i$  and  $i + 1$  for some  $i \in \mathbb{N}$ . Removing all three nodes and readjusting the levels we obtain a rigid binary tree  $\overline{B}$ , satisfying  $|\overline{B}| = |B|$  or  $|\overline{B}| = |B| - 1$ . In the latter case,  $\mathbf{can}$  must satisfy the constraint  $\mathbf{can}(B) = \mathbf{can}(\overline{B})$ . In the former case we define  $\mathbf{can}(B)$  (inductively) by

$$\mathbf{can}(B)(c_1, \dots, c_n) = \mathbf{can}(\overline{B})(c_1, \dots, c_{i-1}, c_i \otimes c_{i+1}, c_{i+2}, \dots, c_n) . \tag{4}$$

where  $(c_1, \dots, c_n)$  is an object or arrow from  $\mathcal{C}^n$ . The arrows of  $\mathcal{B}$  are mapped to iterates of the natural isomorphisms of the premonoidal structure. Thus **can** extends to a mapping

$$\mathbf{can} : \prod_{n=0}^{\infty} (\mathcal{D}(\mathcal{B}_n) \times \mathcal{C}^n) \rightarrow \mathcal{D}(\mathcal{C}) \quad (5)$$

where  $\mathcal{D}(\mathcal{C})$  is the set of all closed finite directed graphs in  $\mathcal{C}$  whose objects are words and arrows are evaluated iterates. The construction of **can** is analogous to the process of diagram projection in the Racah–Wigner category [7]. We define our notion of coherence as follows.

**Definition 1**  $\mathcal{C}$  is  $\mathcal{B}$ -coherent if every diagram  $D \in \mathcal{D}(\mathcal{B})$  gives a commutative diagram  $\mathbf{can}(B)(c_1, \dots, c_{|B|})$  in  $\mathcal{C}$  for all objects  $c_1, \dots, c_{|B|}$  of  $\mathcal{C}^{|B|}$ .

For monoidal categories the coherence groupoid is rooted binary trees (**BTree**) and **can** is that of Mac Lane [9].

### 3. Premonoidal Categories

We begin by considering a natural associativity isomorphism without any conditions such as the Pentagon diagram.

**Definition 2** A premonoidal category is a triple  $(\mathcal{C}, \otimes, \mathbf{a})$  where  $\mathcal{C}$  is a category,  $\otimes : \mathcal{C} \times \mathcal{C} \rightarrow \mathcal{C}$  is a bifunctor and  $\mathbf{a} : \otimes(\otimes \times 1) \rightarrow \otimes(1 \times \otimes)$  is a natural isomorphism for associativity.

The notion of a premonoidal category does not satisfy the Pentagon diagram. Instead we define a natural automorphism which accounts for the difference in the two sides. This amounts to introducing a sixth side which could be inserted anywhere. For reasons which will reveal themselves shortly we define the natural automorphism  $\mathfrak{q} : \otimes(\otimes \times \otimes) \rightarrow \otimes(\otimes \times \otimes)$  according to the hexagonal diagram of figure 2. This is given by composing around the bottom five sides. We call this diagram the  $\mathfrak{q}$ -Pentagon diagram. If you set  $\mathfrak{q} = 1$  you obtain the Pentagon diagram. In the vain of quantum groups [11] one could think of this as a deformation of the Pentagon diagram. We also have a strong version of a premonoidal category. In this case we require  $\mathfrak{q}_{\alpha, \beta, \gamma, \delta} = \mathfrak{q}_{\alpha \otimes \beta, \gamma \otimes \delta}$  for some natural automorphism  $\mathfrak{q} : \otimes \rightarrow \otimes$ . Equivalently we impose the condition that the  $\mathfrak{q}$ -Pentagon diagram holds for  $\mathfrak{q} : \otimes \rightarrow \otimes$ . In this case  $\mathfrak{q}_{\alpha, \beta, \gamma, \delta} = \mathfrak{q}_{\alpha \otimes \beta, \gamma \otimes \delta}$ .

We now turn to the definition of the coherence groupoid for a premonoidal category. The same groupoid describes the strong situation. This groupoid reveals a role for the natural automorphism  $\mathfrak{q}$ . Define **IRBTree** to be the free groupoid whose objects are internally resolved binary trees (denoted IRB tree for short). An IRB tree  $B$  is a rigid binary tree where the internal nodes are assigned a distinct level and the leaves are all assigned the same maximum level  $\overline{B}$ . The length of  $B$  is defined to be the number of leaves. This is given by  $|B| = \overline{B} + 1$ . The internal nodes are labelled by  $0, \dots, \overline{B} - 1$  according to their level. Moreover, an IRB tree is uniquely represented by its internal

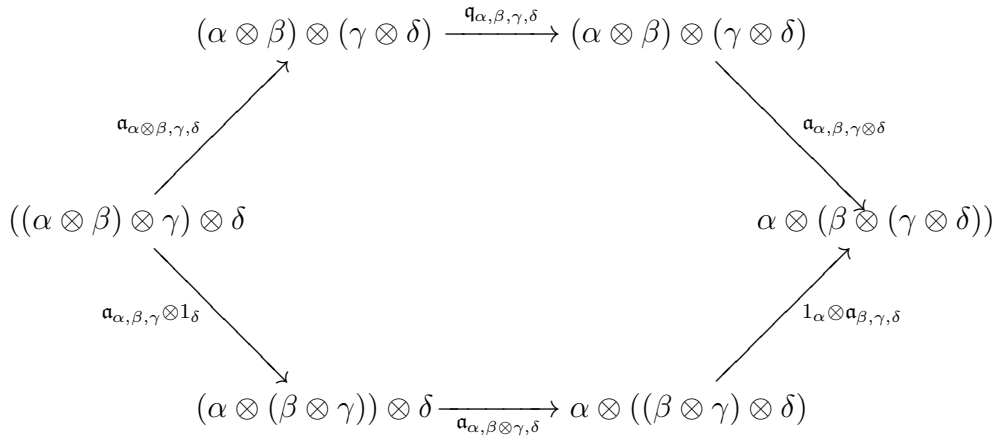


Figure 2. The  $q$ -Pentagon diagram

node levels in the following way. Begin at the left hand most leaf. Trace around the top of the tree. As each internal node is passed at the bottom of a valley write its level down. This produces an ordered sequence of the internal node levels that uniquely describes the IRB tree. An example is given in figure 3. Every permutation of  $012\dots(n - 1)$  represents a unique IRB tree of height  $n$ . Hence there are  $n!$  IRB trees of height  $n$ . The primitive arrows of **IRBTree** are given by formal operations on internal nodes:

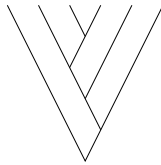


Figure 3. The IRB tree described by 03421.

One may interchange the level of a pair of adjacent branches or reattach an edge. These formal operations are primitive arrows corresponding to iterates of  $\mathbf{a}, \mathbf{a}^{-1}, \mathbf{q}$  and  $\mathbf{q}^{-1}$ ; and are depicted in figure 4. The dashed lines represent attachment sites to the remaining

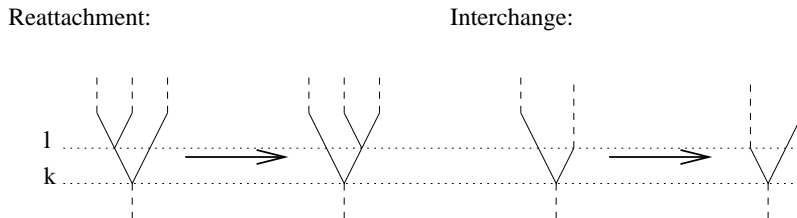


Figure 4. The primitive arrows of **IRBTree** corresponding to iterates of  $\mathbf{a}$  and  $\mathbf{q}$ .

edges and nodes of the binary tree. The node at level  $k$  we call the pivot of the arrow. Recall that the two nodes joining to  $k$  from above are called terminates. Note that for reattachment the lowest terminate level for  $k$  must be greater than  $l$ . We emphasize that we do not require  $l = k + 1$ . If the source for reattachment has a node at level  $l$  on the left (resp. right) the arrow corresponds to an iterate of  $\mathbf{a}$  (resp.  $\mathbf{a}^{-1}$ ). If the source

for interchange has a node at level  $l$  on the right (resp. left) the arrow corresponds to an iterate of  $\mathfrak{q}$  (resp.  $\mathfrak{q}^{-1}$ ). The  $\mathbf{can}$  functor is generated by  $\mathbf{cana} = \mathfrak{a}$ ,  $\mathbf{cana}^{-1} = \mathfrak{a}^{-1}$ ,  $\mathbf{canq} = \mathfrak{q}$  and  $\mathbf{canq}^{-1} = \mathfrak{q}^{-1}$ .

We introduce some useful notation at this point. Let  $B, B'$  be IRB trees. If there is a primitive arrow pivoting about  $k$  between  $B$  and  $B'$  we denote the image under  $\mathbf{can}$  by

$$\text{It}_k^B(\mathfrak{i}) : \mathbf{can}(B) \rightarrow \mathbf{can}(B') , \quad (6)$$

where  $\mathfrak{i}$  is any natural isomorphism of the premonoidal structure. We usually dispense with writing the superscript  $B$ . For example  $\text{It}_2(\mathfrak{a}) = 1 \otimes (\mathfrak{a} \otimes 1)$  for the IRB tree of figure 3.

### Proposition 1

- (i) *Given two IRB trees of height  $n$  then there is a finite sequence of primitive arrows transforming one into the other.*
- (ii) *Every IRB tree of height  $n$  is the source of no more than  $n - 1$  distinct primitive arrows.*
- (iii) *There are  $n!$  distinct IRB trees of height  $n$ .*

*Proof:* (i) We prove by induction on  $n$  that every IRB tree of height  $n$  may be brought into the form  $012\dots(n-1)$ . Consider a binary tree  $a_0a_1\dots a_n$  of height  $n+1$ . If  $a_0 \neq n$  then we may apply the induction hypothesis to  $a_0\dots a_{i-1}a_{i+1}\dots a_n$  where  $a_i = n$  is omitted. In particular there is a sequence of primitive arrows transforming the IRB tree to  $0\dots(i-1)(i+1)\dots(n-1)$ . Hence  $a_0\dots a_n$  can be transformed to  $0\dots(i-1)n(i+1)\dots(n-1)$ . Again the induction hypothesis may be applied to  $1\dots(i-1)n(i+1)\dots(n-1)$  to bring it into the form  $1\dots n$ . Hence  $a_0\dots a_n$  may be brought into the form  $0\dots n$ . If  $a_0 = n$  then by the induction hypothesis we can arrange the last  $n$  terms of  $a_0\dots a_n$  as we wish and hence bring it into the form  $n(n-1)\dots 10$ . The primitive arrow given by the transposition (12) transforms the tree to  $(n-1)n(n-2)\dots 10$ . The first term is not  $n$  so by the first case it may be brought into the form  $01\dots n$ .

(ii) We prove by induction on the height  $n$ . Suppose the hypothesis holds for  $a_0\dots a_{n-1}$ . Consider  $a_0\dots a_n$ . Ignoring  $a_i = n$  we can apply a maximum of  $n$  distinct primitive operations by the induction hypothesis. Any additional operations on  $a_0\dots a_n$  involve a transposition moving  $n$ . There is at most only one possible such primitive operation. Hence there are at most  $n$  distinct primitive arrows with source  $a_0\dots a_n$ .

(iii) This has already been noted.

Each IRB tree  $B$  gives a functor  $\mathbf{can}(B) : \mathcal{C}^{|B|} \rightarrow \mathcal{C}$  given by bracketing according to the binary tree. Note that different IRB trees may map to the same objects and arrows. For example the trees 201 and 102 both correspond to the functor  $(\_\otimes\_\) \otimes (\_\otimes\_)$ . The distinction between the two trees corresponds to a formal weight on the brackets. That is, 201 corresponds to  $(\_\otimes\_)_2 \otimes (\_\otimes\_)_1$  and 102 corresponds to  $(\_\otimes\_)_1 \otimes (\_\otimes\_)_2$ . The primitive arrows of **IRBTree** map to an iterate of one of the natural isomorphisms  $\mathfrak{a}, \mathfrak{a}^{-1}, \mathfrak{q}, \mathfrak{q}^{-1}$ . The  $\mathfrak{q}$ -Pentagon diagram has the underlying **IRBTree** diagram structure



given by figure 5. The notation  $(ij)$  means the natural isomorphism corresponding to the transposition swapping the  $i$ th and  $j$ th positions in the linear ordering.

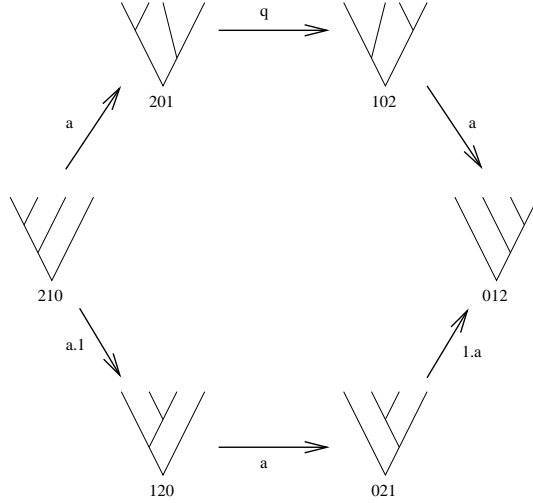


**Figure 5.** The length four diagram in **IRBTree** underlying the  $\mathfrak{q}$ -Pentagon diagram.

**Definition 3** a pseudomonoidal category is a premonoidal category  $(\mathcal{C}, \otimes, \mathbf{a})$  satisfying the two  $\mathfrak{q}$ -Square diagrams of figure 6.

$$\begin{array}{ccc}
 ((\alpha \otimes \beta) \otimes \gamma) \otimes (\delta \otimes \epsilon) & \xrightarrow{\mathfrak{q}_{\alpha \otimes \beta, \gamma, \delta, \epsilon}} & ((\alpha \otimes \beta) \otimes \gamma) \otimes (\delta \otimes \epsilon) \\
 \downarrow \mathbf{a}_{\alpha, \beta, \gamma} \otimes 1_{\delta \otimes \epsilon} & & \downarrow \mathbf{a}_{\alpha, \beta, \gamma} \otimes 1_{\delta \otimes \epsilon} \\
 (\alpha \otimes (\beta \otimes \gamma)) \otimes (\delta \otimes \epsilon) & \xrightarrow{\mathfrak{q}_{\alpha, \beta \otimes \gamma, \delta, \epsilon}} & (\alpha \otimes (\beta \otimes \gamma)) \otimes (\delta \otimes \epsilon) \\
 \\ 
 (\alpha \otimes \beta) \otimes ((\gamma \otimes \delta) \otimes \epsilon) & \xrightarrow{\mathfrak{q}_{\alpha, \beta, \gamma \otimes \delta, \epsilon}} & (\alpha \otimes \beta) \otimes ((\gamma \otimes \delta) \otimes \epsilon) \\
 \downarrow 1_{\alpha \otimes \beta} \otimes \mathbf{a}_{\gamma, \delta, \epsilon} & & \downarrow 1_{\alpha \otimes \beta} \otimes \mathbf{a}_{\gamma, \delta, \epsilon} \\
 (\alpha \otimes \beta) \otimes (\gamma \otimes (\delta \otimes \epsilon)) & \xrightarrow{\mathfrak{q}_{\alpha, \beta, \gamma, \delta \otimes \epsilon}} & (\alpha \otimes \beta) \otimes (\gamma \otimes (\delta \otimes \epsilon))
 \end{array}$$

**Figure 6.** The  $\mathfrak{q}$ -Square diagrams.

If one substitutes for deformativity using the  $\mathfrak{q}$ -Pentagon in the above  $\mathfrak{q}$ -Square diagrams then one sees that these diagrams are actually dodecagons. In this situation the primitive arrows of figure 4 relax the adjacent level requirement. Thus the two  $\mathfrak{q}$ -Square diagrams correspond to the **IRBTree** digrams in figure 7.

We turn now to the coherence of these categories. For a Premonoidal category every  $\mathfrak{q}$  is defined by a sequence of five reattachment arrows under **can**. The  $\mathfrak{q}$  automorphisms

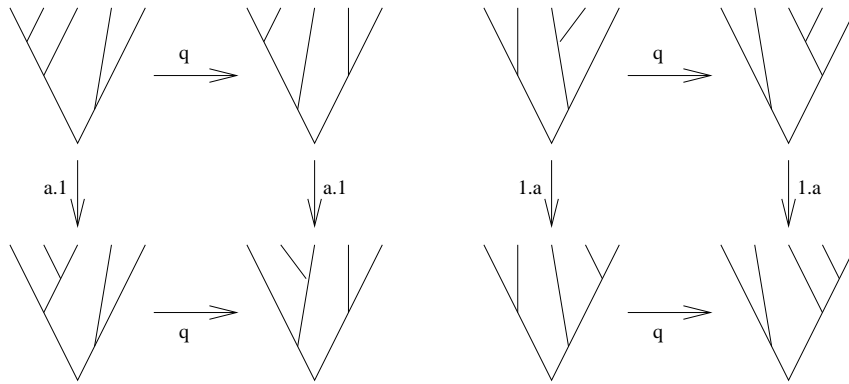


**Figure 7.** The length five diagrams in **IRBTree** underlying the two  $\mathfrak{q}$ -Square diagrams.

may be factored out. Thus all diagrams induced under **can** commute as a result of natural diagrams.

**Theorem 1** *Every pseudomonoidal (resp. strong pseudomonoidal) category  $(\mathcal{C}, \otimes, \mathbf{a})$  is pseudomonoidal coherent (resp. strong pseudomonoidal) coherent if and only if the  $\mathfrak{q}$ -Pentagon diagram and two  $\mathfrak{q}$ -Square diagrams hold.*

*Proof:* Let  $D$  be a diagram in **IRBTree**. Note that each vertex has the same length. Let this length be  $n$ . The rank of a diagram is defined to be the length of any one of its vertices. We prove coherence by induction on diagram rank. The result can be verified explicitly for the ranks 1, 2, 3, 4. The rank four case is given in Appendix A. Suppose the result holds for diagrams of rank  $n+1$ . Let  $a_0, \dots, a_r$  be the vertices for some diagram  $D$  of rank  $n+2$  given by reading around the outside. We identify  $a_{r+1}$  with  $a_0$ . If  $n$  always occurs in the first position of vertex  $a_i$  then  $D$  commutes by naturality and the induction hypothesis. Now suppose that  $n$  does not occur in the first position of some vertices of  $D$ . We divide  $D$  into alternate maximal sections where  $n$  is in the first position alternating with  $n$  is never in the first position. We replace, using the Pentagon diagram, all arrows raising/lowering the first position branch to/from level  $n$ . Now we can and do assume that every arrow moving  $n$  into or out of the first position corresponds to an iterate of  $\mathbf{a}^{-1}$  or  $\mathbf{a}$  respectively.

Let a typical maximal section with  $n$  in the first position be  $a_i \rightarrow \dots \rightarrow a_j$ . Let the arrows  $a_{i-1} \rightarrow a_i$  and  $a_j \rightarrow a_{j+1}$  be  $\text{It}_k(\mathbf{a}^{-1})$  and  $\text{It}_l(\mathbf{a})$  respectively. We show how to replace the sequence  $a_{i-1} \rightarrow \dots \rightarrow a_{j+1}$  with an alternative sequence where the first position is never  $n$ . Moreover, we assume that  $k < l$ . The modification to the other case is obvious. The construction is depicted in figure 8. The sequence of arrows along the top is  $a_{i-1} \rightarrow \dots \rightarrow a_{j+1}$ . The vertical sides of the top left region are identical and keep the position of  $n$  fixed. The bottom arrow of this region moves  $n$  into the first position. This region commutes by the induction hypothesis,  $\mathfrak{q}$ -Square diagrams and naturality. The next region is a natural square that interchanges the levels  $k$  and  $l$ . The bottom and right edges of the centre region is a sequence of arrows keeping  $n$  and  $l$  fixed. The region enclosed always keeps  $n$  fixed and so by hypothesis commutes.

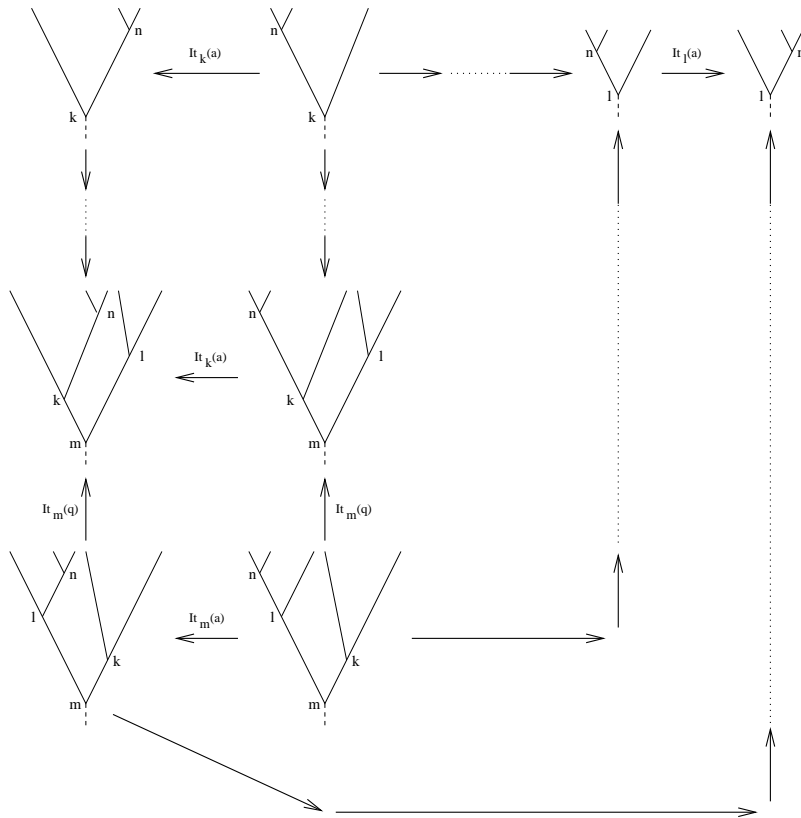


**Figure 8.** Removal of maximal sequence with  $n$  in the first position.

Finally the sequence around the bottom going up the right hand side is a sequence of arrows with  $n$  and  $l$  fixed enclosing the last region. This region commutes by naturality and the induction hypothesis.

If  $n$  is not in a fixed position for every vertex of  $D$ , then we apply the above argument to exclude  $n$  from position two (as well as position one). We repeat this argument inductively for position three, and so on, only stopping when  $n$  is in a fixed position for all vertices of  $D$ . The diagram  $D$  now commutes by the induction hypothesis. This completes the proof.

#### 4. Natural Associativity, Permutations and Linear Orderings

Any natural isomorphism for associativity has a close relationship with the Symmetric groups. The  $\mathfrak{q}$  automorphism that arises accounts for the degenerate nature of the functor  $\otimes(\otimes \times \otimes) : \mathcal{C}^4 \rightarrow \mathcal{C}$ . The Pentagon diagram reflects this degeneracy. The distinction is made in the  $\mathfrak{q}$ -Pentagon diagram. Even if the Pentagon diagram holds the distinction can always be made at the formal level. In a nutshell a premonoidal structure allows one to utilise the symmetric groups and avoid the combinatorics of Catalan numbers. We spell out the precise connection here. A similar relationship, this time between the associahedron and the permutohedron, has been given in Tonks [20].

Let  $\mathcal{LO}_n$  be the groupoid of linear orderings of length  $n$ . The objects are linear

orderings of  $0, 1, \dots, n - 1$  and the arrows are permutations. The groupoid of all linear orderings is given by  $\mathcal{LO} = \coprod_{n=0}^{\infty} \mathcal{LO}_n$ . Let  $F : \mathbf{IRBTree} \rightarrow \mathcal{LO}$  be the functor outlined in the previous section. Each IRB tree is mapped to the sequence of its internal levels and the arrows are mapped to transpositions. Premonoidal and pseudomonoidal coherence (Theorem 1) implies that  $F$  is bijective. Moreover, we can extend the canonical functor to  $\mathcal{LO}$ . This functor is

$$\mathbf{sym} : \mathcal{LO} \rightarrow \prod_{n=0}^{\infty} [\mathcal{C}^n, \mathcal{C}], \tag{7}$$

where  $\mathbf{sym} \circ F = \mathbf{can}$ .

Briefly we consider the construction of  $\mathfrak{q}$ -associahedra. The polytope for words of length five is given in figure 53. This planar diagram folds into the partially-formed truncated octahedron of figure 54. Some faces are missing or halved of this shape. Also there are four vertices that are the source of only two primitive arrows instead of three. This prevents the construction of a polytope. The solution to this dilemma is to use the permutation structure. We summarise in the first few polytopes (or permutahedra) in the following table. Note that because of the  $\mathfrak{q}$ -Pentagon diagram every permutation

$n$	source	$\mathbf{sym}(12)$	$\mathbf{sym}(23)$	polytope
2	0			point
3	01	$\mathfrak{a}^{-1}$		line segment
	10	$\mathfrak{a}$		
4	012	$\mathfrak{a}^{-1}$	$\mathfrak{a}^{-1}$	hexagon
	102	$\mathfrak{a}$	$\mathfrak{a}^{-1}(1.\mathfrak{a}^{-1})\mathfrak{a}$	
	021	$\mathfrak{a}(\mathfrak{a}^{-1}.1)\mathfrak{a}^{-1}$	$\mathfrak{a}$	
	201	$\mathfrak{a}(\mathfrak{a}.1)\mathfrak{a}^{-1}$	$\mathfrak{a}^{-1}$	
	210	$\mathfrak{a}$	$\mathfrak{a}$	
	120	$\mathfrak{a}^{-1}$	$\mathfrak{a}^{-1}(1.\mathfrak{a})\mathfrak{a}$	
5	0123	$\mathfrak{a}^{-1}$	$1.\mathfrak{a}^{-1}$	truncated octahedron
	$\vdots$	$\vdots$	$\vdots$	

**Table 1.** The generators of  $\mathcal{LO}_n$  where  $2 \leq n \leq 5$ .

under  $\mathbf{sym}$  can be described by a sequence of iterates of  $\mathfrak{a}$ .

### 5. $\mathfrak{q}$ -Pseudomonoidal Categories

The  $\mathfrak{q}$  natural automorphism for pseudomonoidal categories was found to behave (at the formal level at least) as an interchange of the internal node level. In this section we extend this idea to include the interchange of leaf levels as well.

**Definition 4** A  $\mathfrak{q}$ -pseudomonoidal category is a quadruple  $(\mathcal{C}, \otimes, \mathfrak{a}, \mathfrak{q})$  where  $\mathcal{C}$  is a category,  $\otimes : \mathcal{C} \times \mathcal{C} \rightarrow \mathcal{C}$  is a bifunctor,  $\mathfrak{a} : \otimes(\otimes \times 1) \rightarrow \otimes(1 \times \otimes)$  and  $\mathfrak{q} : \otimes \rightarrow \otimes$  are

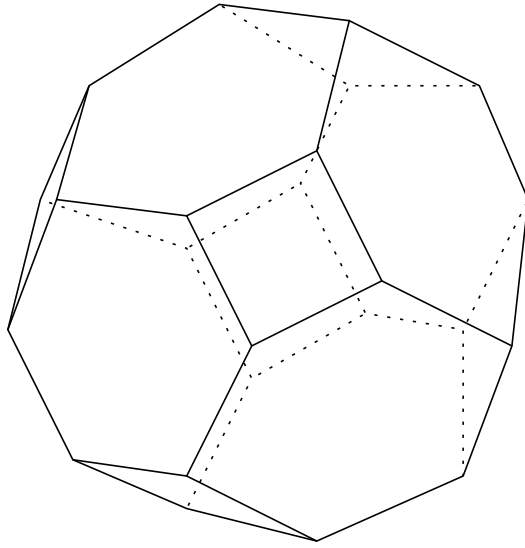


**Figure 9.** A truncated octahedron.

natural isomorphisms satisfying  $(\mathcal{C}, \otimes, \mathbf{a}, \mathbf{q})$  is strong pseudomonoidal and the Dodecagon diagram (figure 10) and the two Quaddecagon diagrams (figures 11 and 12) hold.

Note that we sometimes use a dot as an abbreviation of  $\otimes$  (as in figures 11 and 12) and often dispense with subscripts on the natural isomorphisms.

In order to understand the Dodecagon and Quaddecagon diagrams we need to understand the underlying combinatorics. Define a resolved binary tree or RB tree to be a rigid binary tree where every node is assigned a distinct level. We represent an RB tree by a finite sequence of levels as follows. Tracing around the top of the tree beginning at the left hand side leaf, we generate a sequence of all the node levels,  $a_1, a_2, \dots, a_{2n-1}$ , where  $n$  is the length of the tree. We also write this sequence in the exploded form

$$\begin{array}{cccccccc} a_1 & & a_3 & & a_5 & \cdots & a_{2n-3} & & a_{2n-1} \\ & & a_2 & & a_4 & \cdots & & & a_{2n-2} \end{array} \quad (8)$$

The bottom row contains the internal node levels and the top the leaf levels. The levels satisfy  $a_{2i} < a_{2i-1}, a_{2i+1}$  for all  $i = 1, 2, \dots, n - 1$ . Moreover, any such format of the numbers  $0, 1, \dots, 2n - 1$  obeying this condition uniquely determines an RB tree. We let **RBTree** denote the free groupoid of RB trees. The objects are RB trees. The arrows are generated from the primitive operations for reattachment of adjacent edges (corresponding to associativity) and interchange of level (corresponding to  $\mathbf{q}$ ). These operations are the obvious extensions of the primitive operations of **IRBTree** (figure 4). The degree of connectedness and size of **RBTree** is given by Proposition 2.

**Proposition 2**

- (i) Given two RB trees of length  $n$  then there is a finite sequence of primitive arrows transforming one into the other.
- (ii) Every RB tree of length  $n$  is the source of no more than  $2(n - 1)$  distinct primitive arrows.

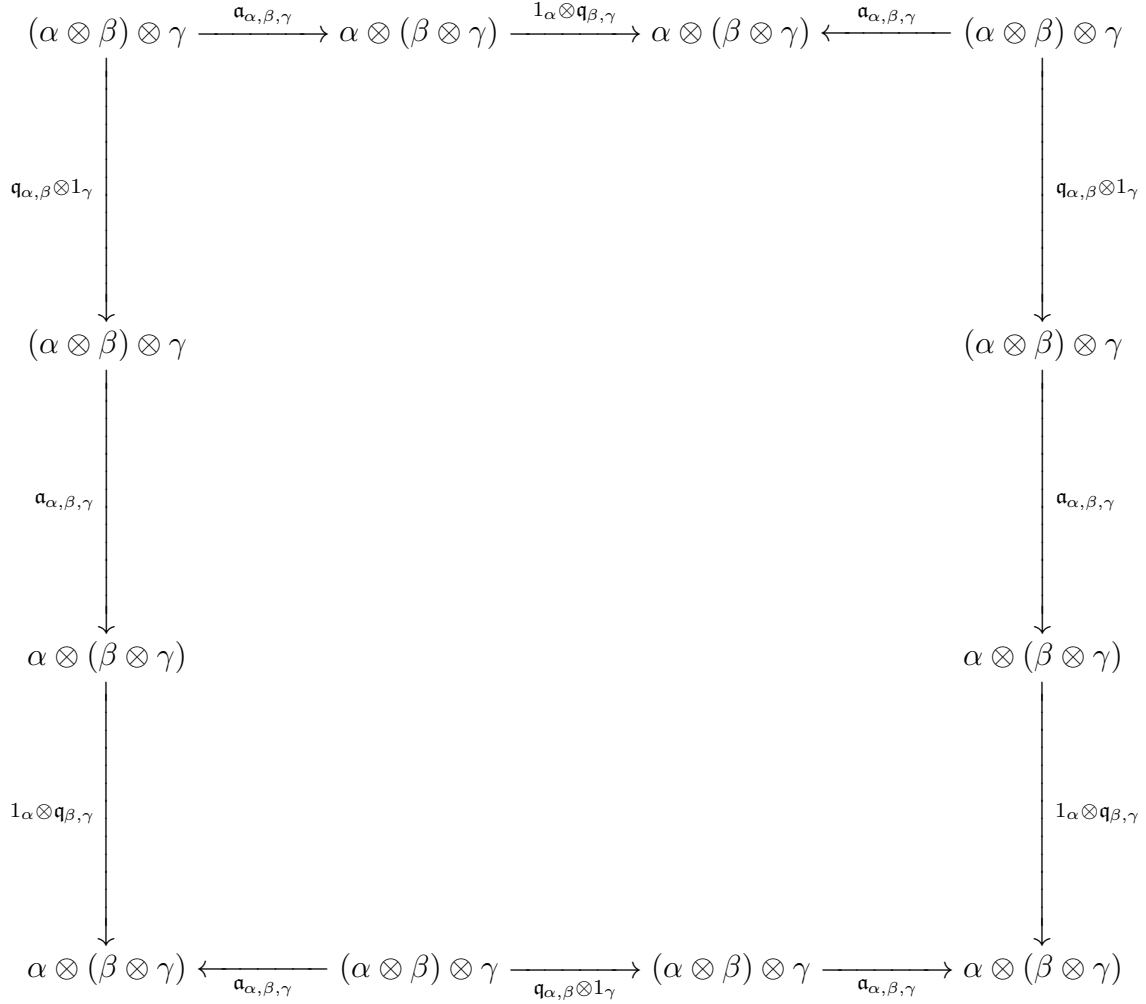


Figure 10. The Dodecagon diagram.

(iii) Let  $T(m)$  be the number of RB trees of length  $m$ .  $T(n)$  satisfies the recursive formula

$$T(n) = \sum_{m=1}^{n-1} \binom{2n-2}{2m-1} T(m)T(n-m), \quad T(1) = 1. \quad (9)$$

*Proof:* (i) We use the principle of strong induction. Clearly the result holds for  $n = 2$ . Suppose it holds for  $n$  and consider a RB tree  $B$  of length  $n + 1$ . We will show that it can be brought into the standard form  $\begin{matrix} 1 & 3 & 5 & \cdots & 2n-2 & & 2n-1 \\ 0 & 2 & 4 & \cdots & 2n-3 & & 0 \end{matrix}$ . It follows from this, because the arrows are invertible, that any two trees that can be brought into standard form can also be transformed one to the other. If  $B$  begins  $\begin{matrix} 1 \\ 0 \end{matrix}$  then the remaining portion may be transformed into standard form by the induction hypothesis. If  $B$  ends  $\begin{matrix} \cdots \\ 0 \end{matrix}$  then  $B$  may be brought into the form  $\begin{matrix} 3 & 5 & \cdots & 2n-2 & & 2n-1 & 1 \\ 2 & 4 & \cdots & 2n-3 & & 0 & 0 \end{matrix}$ . Interchanging 1 and 2 then  $B$  falls in the next case to be considered.

The only other case that can occur is when 0 and 1 are both in the bottom row of  $B$ . We suppose that 1 is to the right of the 0. If not then one simply interchanges them and continues. Let  $m$  be the smallest level to the left of 0. Hence  $1, \dots, m-1$  are to the right of 0. If  $m < 2n+1$  then  $m+1$  occurs in  $B$ . If it occurs to the right of 0 then by the induction

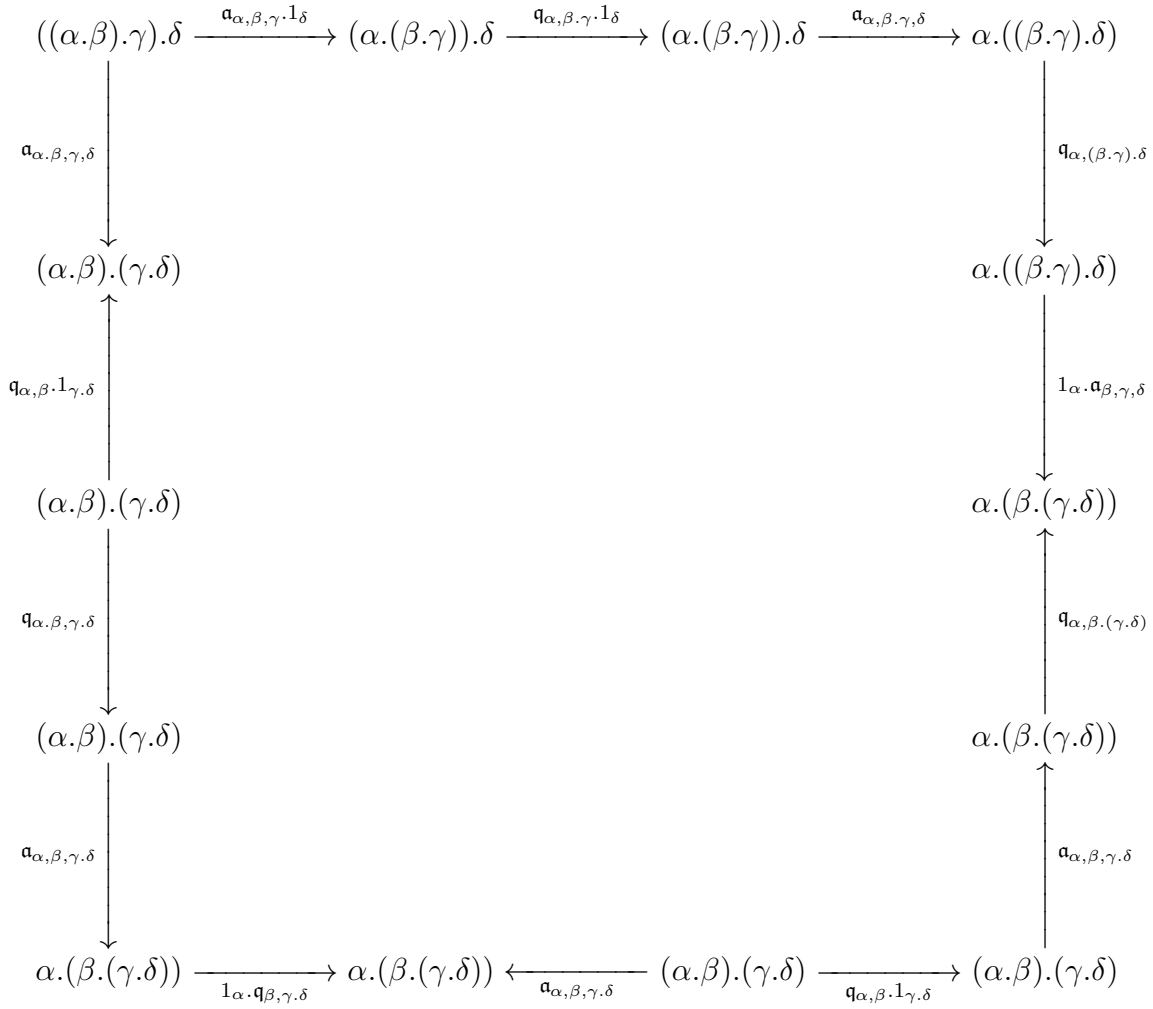
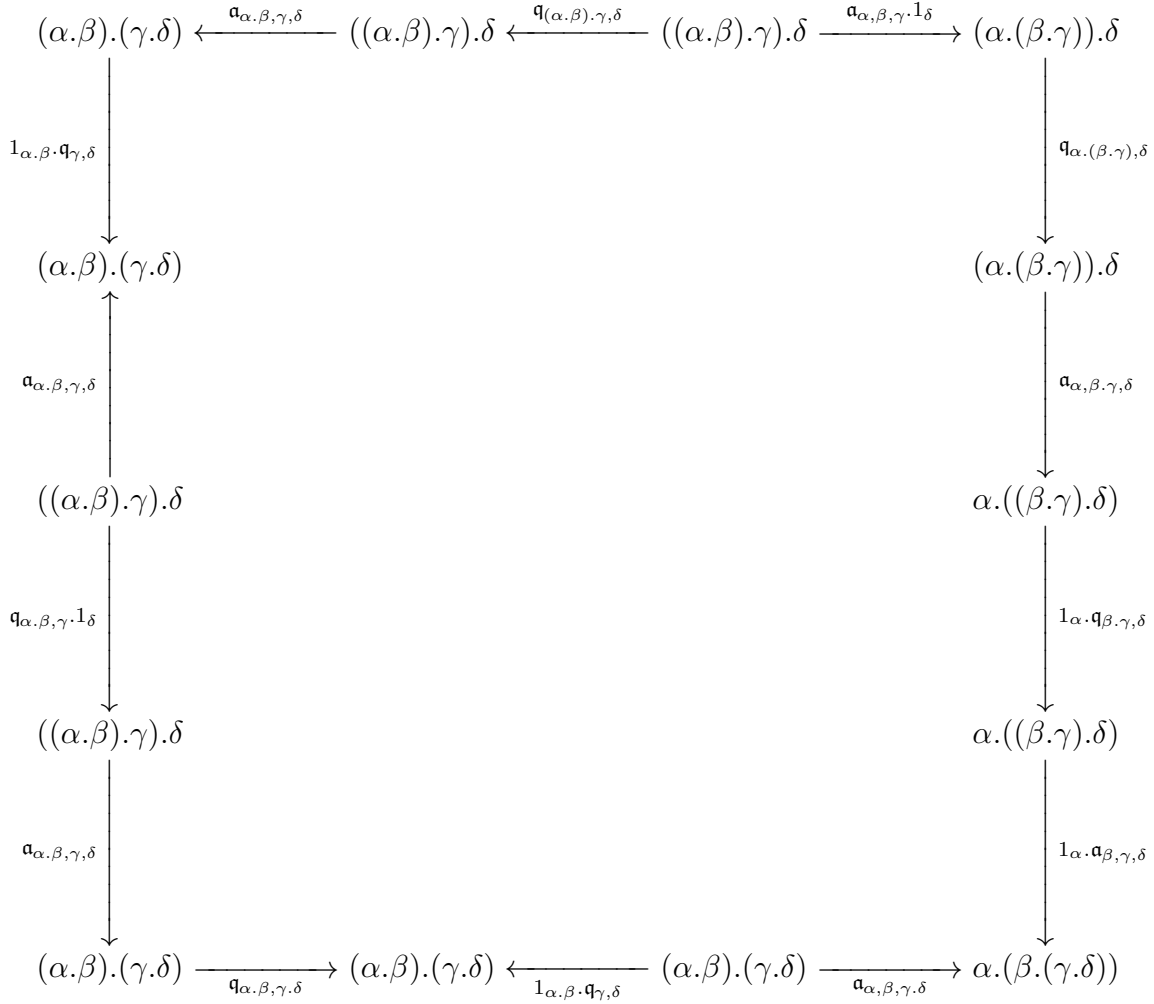


Figure 11. The first Quaddecagon diagram.

hypothesis applied to  $1, \dots, m-1$  we bring  $B$  into the form  $\dots m \dots 0(m+1)1 \dots$ . To this we apply the sequence of primitive operations: interchange 0 and 1, then interchange  $m$  and  $m+1$ , and finally interchange 0 and 1. Thus  $B$  is in the form  $\dots (m+1) \dots 0m1 \dots$ . Hence the smallest level to the left of 0 is increased to  $m+1$ . In the other situation  $m+1$  is to the left of 0 and on the bottom row. Applying the induction hypothesis to  $1, \dots, m-1$  we bring  $B$  into the form  $\dots m \dots 0 \dots (m-1) \dots (m-2) \dots \dots 2 \dots 1 \dots$  where  $1, \dots, m-1$  are internal (and on the bottom row in the exploded form). Next we apply the sequence of primitive operations: Interchange 0 with 1, then interchange 1 with 2, continuing this process until the interchange  $m-2$  with  $m-1$ . Now  $B$  is in the form  $\dots m \dots (m-1) \dots \dots 2 \dots 1 \dots 0 \dots$  and  $0, \dots, m$  are all internal. Next we reverse the sequence of primitive operations: Interchange  $m$  with  $m-1$ , then interchange  $m-1$  with  $m-2$ , continuing this process until the interchange 0 with 1. Now  $1, \dots, m$  are all to the left of 0 and the smallest level to the left of 0 has been increased to  $m+1$ . Hence, whenever  $m < 2n+1$  we continue to apply the above procedures terminating when  $m$  has been increased to  $2n+1$ . Hence  $B$  is of the form  ${}^{2n+1}_0 \dots$ . By the induction hypothesis applied to  $1, \dots, 2n$  we bring  $B$  into the form  ${}^{2n+1}_0 {}^2_1 \dots$ . Now we apply the primitive



**Figure 12.** The second Quaddecagon diagram.

operations: Interchange 0 and 1, then interchange  $2n + 1$  and 2, then interchange 0 and 1 again, and finally interchange 1 and 2. This brings  $B$  into the form  ${}^1_0 2n+1 \dots$  which we have already shown can be brought into standard form. This completes the proof of (i).

(ii) This is proved by a strong induction argument. The result is true for  $n = 2$ . Suppose it is true for all RB trees of length less than or equal to  $n$ . Any RB tree  $B$  of length  $n + 1$  can be divided at 0 into two trees of length  $m$  and  $n - m$  respectively. A maximum of two primitive operations can pivot about 0 and applying the induction hypothesis to both trees we get an upper bound of  $2(m - 1) + 2(n - m) + 2 = 2n$  for the maximum number of primitive operations on  $B$ .

(iii) An RB tree of length  $n$  has  $2n - 1$  levels with the first level occupied by the root. We divide the tree into left hand and right hand components. If the left hand tree is of length  $m$  then the right hand tree is of length  $n - m$  where  $0 < m < n$ . The left hand tree will occupy  $2m - 1$  levels. There are  $\binom{2n-2}{2m-1}$  ways of choosing the levels for this tree. Hence there are  $\binom{2n-2}{2m-1} T(m)$  configurations of the left hand tree. Moreover, the right hand tree is assigned the remaining levels and it can be configured  $T(n - m)$  ways.



Hence there are  $\binom{2n-2}{2m-1} T(m)T(n-m)$  RB trees with  $m$  leaves to the left of the root. The result follows by summing over the different possibilities for  $m$ .

One should note that the operations corresponding to  $\mathfrak{q}$  are not restricted to consecutive levels. This is because Proposition 2(i) fails if such a restriction is enforced. Without this property then one would have no means of constructing a coherent natural isomorphism between any two isomorphic words composed of the same letters. The number of RB trees of length  $n$  can be calculated by the recursion formula of Proposition 2(iii). The first six are given in table 2. The recursive formula for  $T(n)$  generates the

n	T(n)
1	1
2	2
3	16
4	272
5	7936
6	353792

**Table 2.** The number of RB trees of length  $n$ .

tangent (or Zag) numbers given by the  $n$ th term of the expansion in  $\tan x$  thus

$$\tan x = \sum_{n=1}^{\infty} T(n) \frac{x^{2n-1}}{(2n-1)!}. \tag{10}$$

Explicitly,

$$T(n) = \left. \frac{d^{2n-1}}{dx^{2n-1}} \tan x \right|_{x=0}. \tag{11}$$

Alternatively  $T(n)$  is given by the number of up down permutations on  $2n-1$  numbers, see Millar *et. al.* [21].

The underlying **RBTree** diagrams for the Dodecagon and Quaddecagon diagrams are given by figures 13, 14 and 15. The  $\mathfrak{q}$ -Pentagon is given by figure 5 where the leaf levels occupy the levels above the pivot levels. Observe that as a direct result of Theorem 1 the Dodecagon and Quaddecagon diagrams all commute whenever all the leaves in figures 13, 14 and 15 are replaced by branches.

In general when some of the leaf levels are less than some of the branch levels constructing a sequence of arrows between any two RB trees is quite involved. We give an algorithm, called Left Reduction, which constructs a sequence of primitive arrows reducing any vertex to reduced form. Reduced form is where all the branch levels are less than all the leaf levels. In fact it does a little more than this as we shall see. This algorithm plays a central role in the proof of  $\mathfrak{q}$ -pseudomonoidal coherence. Given a RB tree,  $B$ , the algorithm constructs a sequence of primitive arrows reorganising  $B$  into a left-reduced RB tree. We say an RB tree is  $l$ -left reduced if the left terminate node of  $l$  is not a branch at level  $l+1$  and every level less than  $l$  (excluding the root) is a branch and the left terminate for the next level down. The tree is called left reduced

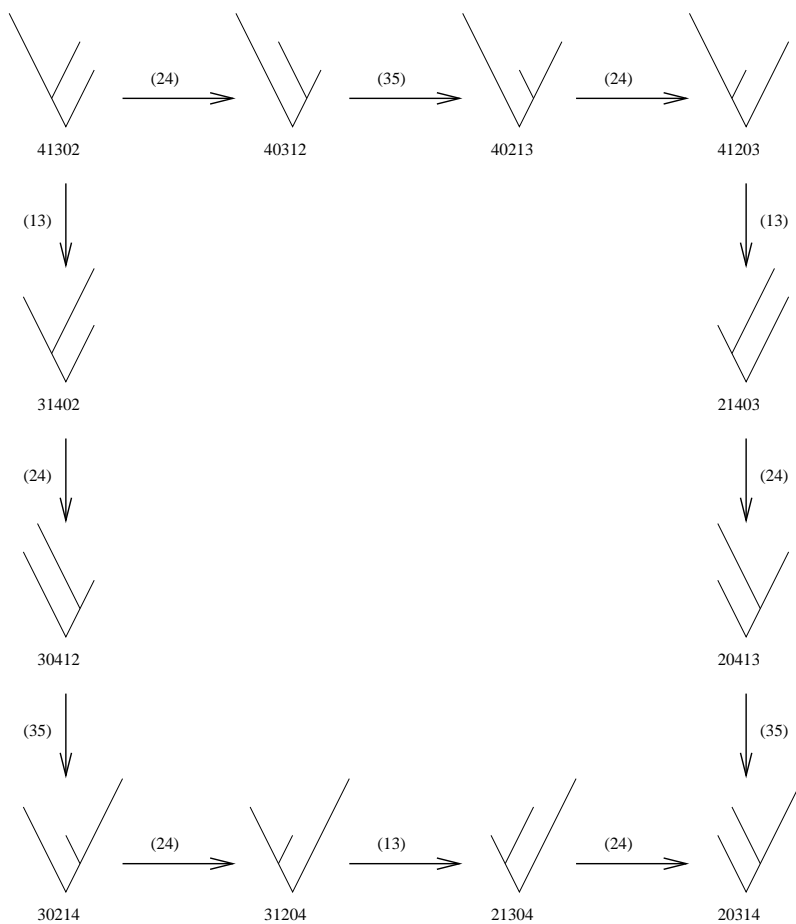


**Figure 13.** Diagram in **RBTree** underlying the Dodecagon diagram.

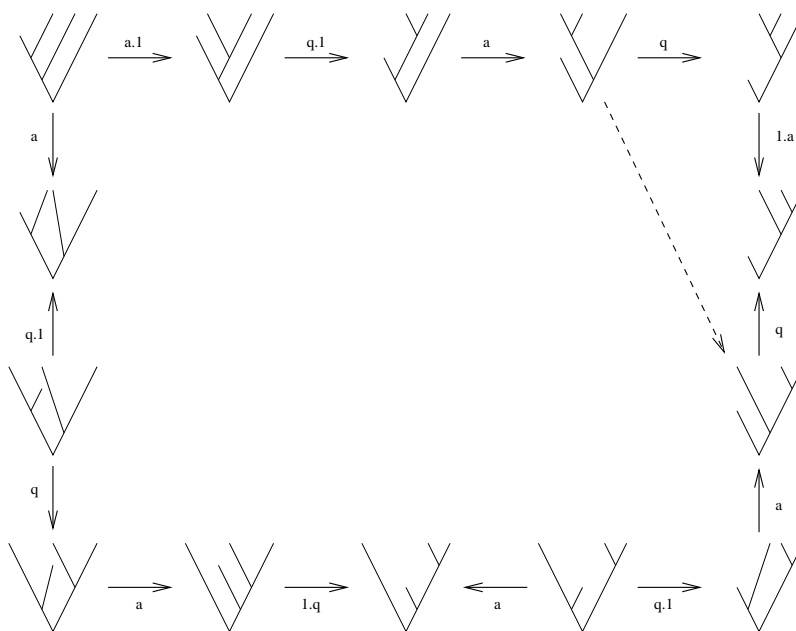


**Figure 14.** Diagram in **RBTree** underlying the First Quaddecagon diagram.

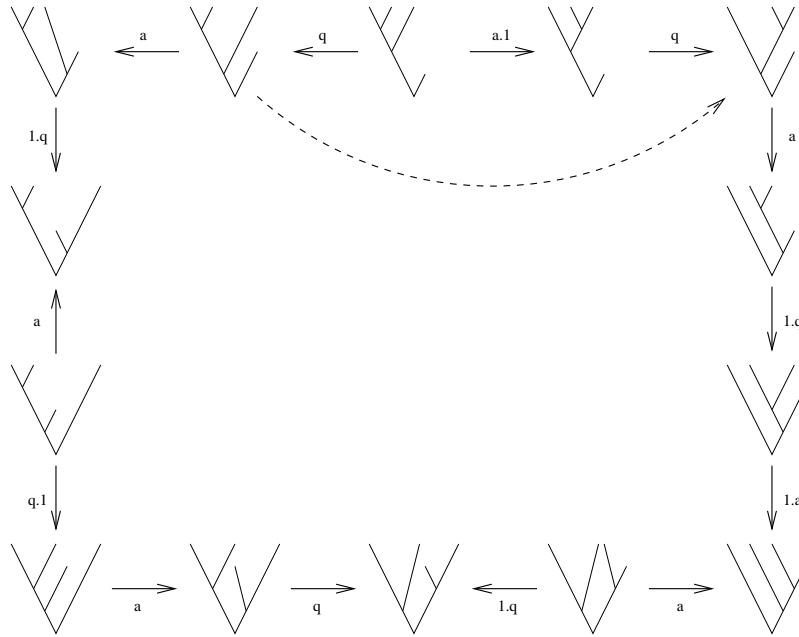


**Figure 15.** Diagram in **RBTree** underlying the Second Quaddecagon diagram.

if it is  $|B|$ -left reduced or equivalently if the underlying IRB tree is  $|B|(|B| - 1) \dots 210$ . We introduce some further useful notation. A  $k$ -cut is where we draw a horizontal line between the levels  $k - 1$  and  $k$ . Every node at a level greater than  $k - 1$  that is a terminate for a node at a level less than  $k$  is called a  $k$ -cut node. The line segment between these two nodes cuts the horizontal line. If the lines in our binary tree do not cross then the  $k$ -cut nodes have a unique order along this line. We number them from right to left beginning at 0. An example is given in figure 16. Note that for an  $l$ -cut of

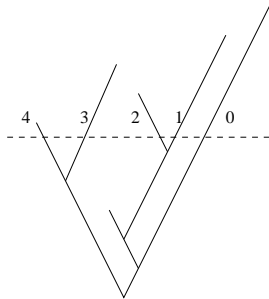


**Figure 16.** A 6-cut for the RB tree 6480327591(10).

an  $l$ -left reduced RB tree the  $l$ -cut node positions (except for the highest positioned) are given by the level of the node for which each is a terminate.

We now give the Left Reduction algorithm for constructing a sequence of primitive arrows reducing an RB tree,  $B$ , to a left reduced RB tree. Note that  $\mathbf{q}$  and  $\mathbf{q}^{-1}$  will not be distinguished. The levels of the terminates tells you which one is meant. The algorithm begins with the sequence  $B$  which is composed of no arrows. The algorithm proceeds inductively from the last object of the sequence.

**The Left Reduction Algorithm**

- (i) Locate the largest  $l > 0$  in the last object of the sequence such that this object is  $l$ -left reduced.
- (ii) If level  $l + 1$  is a left terminate of  $l$  then (it is a leaf and) interchange about the pivot  $l$ .
- (iii) Let  $r$  be the level with  $l + 1$  as a terminate. Let  $b$  be the branch level for which the lowest levelled  $l$ -cut branch node is a terminate. If no such  $b$  exists then go to (x).
- (iv) If  $r < b$  apply the sequence  $\prod_{i=0}^{b-r-1} \text{It}_{r+i}(\mathbf{a}^{-1}(1.\mathbf{q})\mathbf{a})$ .
- (v) If the  $l$ -cut node attached to  $b$  is the left terminate of  $l$  then ( $b = l$  and) apply  $\text{It}_l(\mathbf{q})$ . Thus the  $l$ -cut node has been lowered to level  $l + 1$ .
- (vi) If  $r > b$  apply the sequence  $\prod_{i=1}^{r-b} \text{It}_{r-i}(\mathbf{a}^{-1}(1.\mathbf{q})\mathbf{a})$ . Thus the  $l$ -cut node  $b$  has been lowered to level  $l + 1$ .
- (vii) If  $b = l$  then apply  $\text{It}_l(\mathbf{a}^{-1})$  if required to bring into  $(l + 1)$ -left reduced form and go to (x).
- (viii) Apply  $\prod_{j=1}^{l-b} \prod_{i=l-b-j}^{l-b-i} \text{It}_{b+i}(\mathbf{a})$ .
- (ix) Apply  $\prod_{j=1}^{l-b+1} \prod_{i=l-b-j+1}^{l-b-i+1} \text{It}_{b+i}(\mathbf{a}^{-1})$ . Thus the  $l$ -cut node  $b$  has been lowered to level  $l + 1$ .
- (x) If  $l < |B| - 3$  then go to (i).

A schematic diagram is given in figure 17 for this algorithm. The following lemma gives us an upper bound on the algorithms complexity.

**Lemma 1** *Given an RB tree of length  $n$  then the above algorithm reduces it to a left reduced RB tree using a sequence of  $O(n^2)$  primitive arrows.*

*Proof:* Assuming the worst case then for an  $l$ -cut RB tree we count the maximum number of primitive arrows: The worst case is the sequence of steps (i),(iv),(v),(vii),(ix). The maximum number for each is 0,  $3l$ , 1,  $l$  and  $l + 1$  respectively. Summing over  $l$  from 1 to  $n - 2$  we generate a sequence of primitive arrows with at most

$$\sum_{l=1}^{n-2} (5l + 2) = \frac{(5n - 1)(n - 2)}{2} \quad (12)$$

arrows. This is  $O(n^2)$ .

We are now in a position to prove a coherence result for  $\mathbf{q}$ -pseudomonoidal categories.

**Theorem 2** *If  $\mathcal{C}$  is a category,  $\otimes : \mathcal{C} \times \mathcal{C} \rightarrow \mathcal{C}$  a bifunctor and  $\mathbf{a} : \otimes(\otimes \times 1) \rightarrow \otimes(1 \times \otimes)$  and  $\mathbf{q} : \otimes \rightarrow \otimes$  natural isomorphisms then this structure is  $\mathbf{q}$ -pseudomonoidal coherent if and only if the  $\mathbf{q}$ -Pentagon diagram (figure 2), the  $\mathbf{q}$ -diagrams (figure 6), the Dodecagon diagram (figure 10) and the Quaddecagon diagrams (figures 11 and 12) all commute.*

*Proof:* The proof is by induction on the length  $n$  of RB trees. We define the rank of a diagram in **RBTree** to be the length of any one of its vertices. The result holds

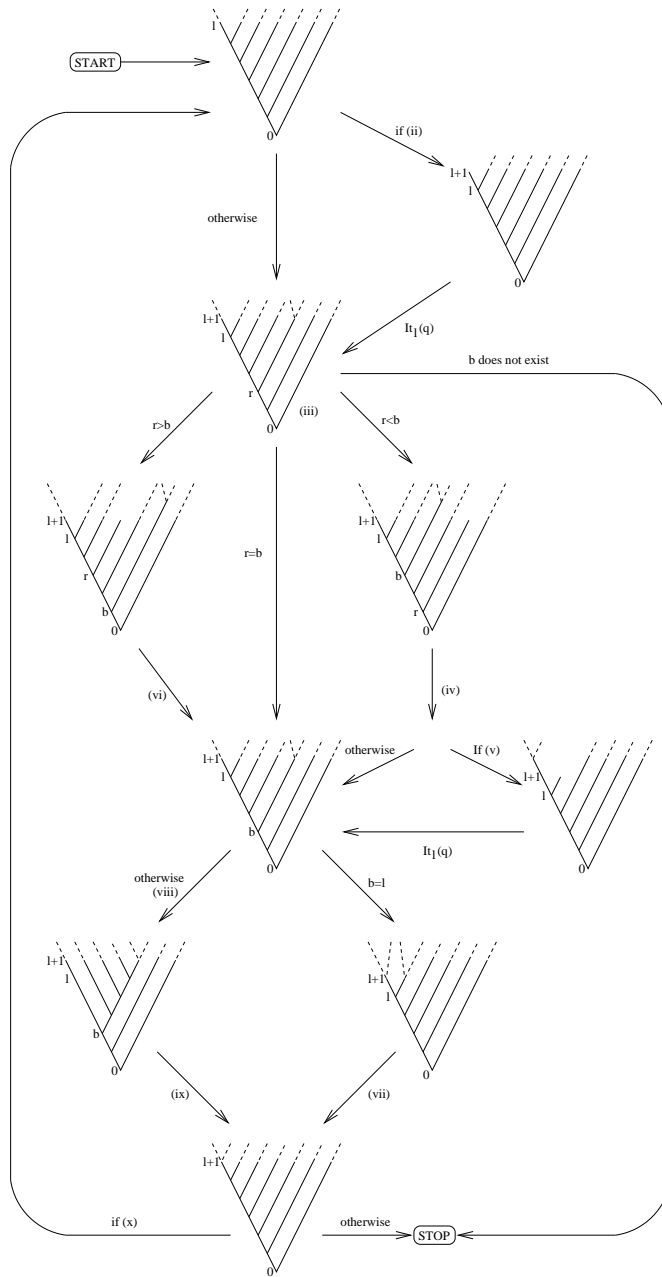
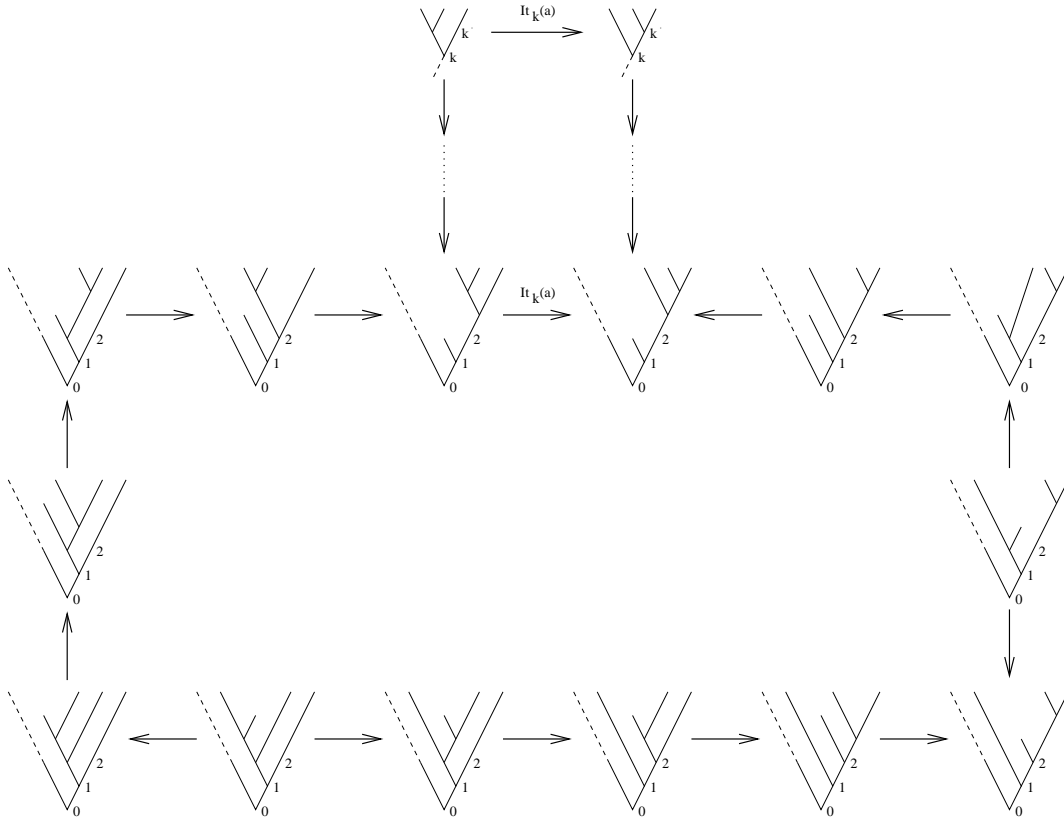


Figure 17. A schematic diagram of the Left Reduction algorithm.

for  $n = 1, 2, 3$ . Suppose the theorem holds for diagrams of length  $n \geq 3$ . Let  $D$  be a diagram of length  $n + 1$ . The induction step is in two parts. Firstly we show that the diagram  $D$  is equivalent to a diagram of the same length whose vertices are all in reduced form. A vertex is in reduced form if all the branch levels are below all the leaf levels. A diagram is in reduced form if all of its vertices are in reduced form. Secondly we show that all diagrams in reduced form of length  $n + 1$  commute.

**Part One:** Let the vertices of  $D$  be  $a_0, \dots, a_r$  reading around the outside and put  $a_{r+1} = a_0$ . We substitute certain arrows that would cause problems further on in the proof. We replace all arrows  $It_k(\mathbf{a}), It_k(\mathbf{a}^{-1}) : a_i \rightarrow a_{i+1}$  for which the lowest terminate

level of  $k$  is the highest branch of  $a_i$ . We demonstrate how to substitute for  $\text{It}_k(\mathbf{a})$ . The substitution for  $\text{It}_k(\mathbf{a}^{-1})$  follows by reversing all arrows. Let  $k'$  be the left terminate level of  $k$ . We assume that  $k'$  is not the left hand most branch point. Consider the diagram of figure 22. We construct two identical sequences of arrows  $a_i \rightarrow \dots \rightarrow b_i$  and



**Figure 18.** Diagram for removing the arrow  $\text{It}_k(\mathbf{a}) : a_i \rightarrow a_{i+1}$ .

$a_{i+1} \rightarrow \dots \rightarrow b_{i+1}$  represented by the vertical sides of the top region. This sequence is constructed such that the branches  $k$  and  $k'$  and their terminates remain fixed by each arrow and the highest branch level for each vertex is  $k'$ . The vertices  $b_i$  and  $b_{i+1}$  are of the form indicated by diagram. The arrow  $b_i \rightarrow b_{i+1}$  is  $\text{It}_k(\mathbf{a})$  and the region enclosed commutes by the induction hypothesis and naturality. We replace the arrow  $b_i \rightarrow b_{i+1}$  by the fourteen vertex diagram as indicated. The this region commutes by the first Quaddecagon diagram (figure 14). Thus we substitute for  $\text{It}_k(\mathbf{a})$  using the perimeter of the two regions of the diagram in figure 22. If  $k'$  is the left hand most branch then a similar substitution is performed using the second Quaddecagon diagram.

We assume that the diagram  $D$  has been substituted as outlined above. For each  $i$  we construct a sequence of arrows  $a_i \rightarrow \dots \rightarrow b_i$  using the Left Reduction algorithm. Next we construct a sequence of arrows  $b_i \rightarrow \dots \rightarrow b_{i+1}$  composed of reduced vertices such that the region enclosed commutes. This will prove the claim of part one.

Let  $k$  be the pivot of  $a_i \rightarrow a_{i+1}$  then this arrow is either  $\text{It}_k(\mathbf{a})$  or  $\text{It}_k(\mathbf{q})$ . (The inverses are accounted for by reversing arrows.) Consider the arrow  $\text{It}_k(\mathbf{a}) : a_i \rightarrow a_{i+1}$ .

Let  $k'$  be the left terminate of  $k$ . The level  $k'$  is not the level of the highest branch. We apply the Left Reduction algorithm to  $a_i$  and  $a_{i+1}$  until we reach the last cycle. At this point the last vertices of the sequences constructed coincide. Moreover, the region enclosed commutes by the induction hypothesis since the highest branch and its terminates are the same in all vertices. Hence  $b_{i+1} = b_i$ .

Now consider the arrow  $\text{It}_k(\mathbf{q}) : a_i \rightarrow a_{i+1}$ . Let  $a$  and  $b$  be the terminates of  $k$  with  $a$  to the left of  $b$ . We allow the algorithm to cycle through until the last cycle. Let  $a_i \rightarrow \cdots \rightarrow c_i$  and  $a_{i+1} \rightarrow \cdots \rightarrow c_{i+1}$  be the partially constructed sequences up until the last cycle of the algorithm is applied.  $c_i$  and  $c_{i+1}$  are  $l$ -left reduced. The highest branch either has  $a$  and  $b$  or neither as terminates. Let  $k'$  be the pivot of  $a$  and  $b$  in  $c_i$  (and hence  $c_{i+1}$ ). In the former case the interchange of  $a$  and  $b$  is natural with respect to the arrows of the partial sequences. Hence  $\text{It}_{k'}(\mathbf{q}) : c_i \rightarrow c_{i+1}$  is a primitive arrow. The region enclosed commutes by the induction hypothesis. In the latter case neither the levels of the terminates for highest branch are altered nor is their pivot reattached. Hence the primitive sequence  $\text{It}_{k'}(\mathbf{a}^{-1}(1, \mathbf{q})\mathbf{a}) : c_i \rightarrow c_{i+1}$  encloses a region that is a diagram of length  $n$  that commutes by the induction hypothesis.

It remains to show the commutativity of the region enclosed by the final cycle of the Left Reduction algorithm. The  $c_i$  fall into three cases:

Case (a):  $a \leq l$  or  $b \leq l$ . One (or both) of  $a, b$  have been absorbed and  $c_{i+1} = c_i$ . Hence  $b_{i+1} = b_i$ .

Case (b):  $a$  and  $b$  are terminates of the highest branch. The arrow  $\text{It}_{k'}(\mathbf{q}) : c_i \rightarrow c_{i+1}$  commutes with steps (i) to (viii). Applying these steps we construct sequences  $c_i \rightarrow \cdots \rightarrow d_i$  and  $c_{i+1} \rightarrow \cdots \rightarrow d_{i+1}$ . The arrow  $\text{It}_{k'}(1, \mathbf{q})$  is natural with respect to these sequences. Moreover,  $d_i, d_{i+1}$  have highest branch at level  $l + 1$  with terminates the leaves  $a$  and  $b$ . The arrow  $\text{It}_l(\mathbf{q}) : d_i \rightarrow d_{i+1}$  encloses a region that commutes by naturality. Use the final step of the algorithm to generate the sequences  $d_i \rightarrow \cdots \rightarrow b_i$  and  $d_{i+1} \rightarrow \cdots \rightarrow b_{i+1}$ . Hence these three sequences compose to give a sequence  $b_i \rightarrow \cdots \rightarrow d_i \rightarrow \cdots \rightarrow d_{i+1} \rightarrow \cdots \rightarrow b_{i+1}$  where every vertex is in reduced form.

Case (c):  $a$  and  $b$  are attached to different pivots. Note that it is only possible for one of  $a$  and  $b$  to be a branch. We continue the algorithm through to step (vii). Let  $c_i \rightarrow \cdots \rightarrow d_i$  and  $c_{i+1} \rightarrow \cdots \rightarrow d_{i+1}$  be the sequences constructed. Let  $k$  be the pivot of the branch at the  $l + 1$  level in  $d_i$  (and hence  $d_{i+1}$ ). There exists a sequences of primitive arrows  $c_i \rightarrow \cdots \rightarrow c_{i+1}$  and  $d_i \rightarrow \cdots \rightarrow d_{i+1}$  that do not reattach the highest branch nor interchange its terminates. Hence the regions  $a_i a_{i+1} c_{i+1} c_i$  and  $c_i c_{i+1} d_{i+1} d_i$  commute by the induction hypothesis and naturality. Use the final steps of the algorithm to generate the sequences  $d_i \rightarrow \cdots \rightarrow b_i$  and  $d_{i+1} \rightarrow \cdots \rightarrow b_{i+1}$ . Hence these three sequences compose to give a sequence  $b_i \rightarrow \cdots \rightarrow d_i \rightarrow \cdots \rightarrow d_{i+1} \rightarrow \cdots \rightarrow b_{i+1}$  where every vertex is in reduced form.

**Part Two:** We now prove the second step which is that a diagram  $D$  of length  $n + 1 \geq 5$  whose vertices are in reduced form commutes. We label the leaf levels using an  $(n + 1)$ -cut. The leaf  $v$  is assigned the number  $2n - 1 - l(v)$ . This gives  $\mathbf{q}$  the action of a permutation on the leaf levels. Since  $D$  is in reduced form we are restricted to those

leaves that interchange branch levels and those that interchange leaf levels. the former we call terminal arrows and the latter internal arrows. The latter we will show allow us to construct generators for the permutation group  $S_{n+1}$ . If  $D$  contains only internal arrows then  $D$  commutes by Theorem 1.

Suppose that  $D$  contains at least one terminal arrow. We partition  $D$  into sequences of arrows such that each sequence has exactly one arrow for interchange of leaf levels. Let a typical partition sequence be  $a_m \rightarrow \dots \rightarrow a_p$ . We will show that any alternative sequence  $b_0, \dots, b_q$  with  $b_0 = a_m$  and  $b_q = a_p$  containing only one interchange of leaf levels encloses a region that commutes. Suppose  $a_k \rightarrow a_{k+1}$  and  $b_l \rightarrow b_{l+1}$  are the interchanges of leaf levels. The levels they interchange are identical and occur in the same adjacent positions. Hence there are sequences of internal arrows from  $a_k$  to  $b_l$  and  $a_{k+1}$  to  $b_{l+1}$  such that the region enclosed commutes by naturality. This is depicted in figure 19. Moreover, the regions  $a_m a_k b_l b_0$  and  $a_p a_{k+1} b_{l+1} b_q$  commute. Hence the two sequences

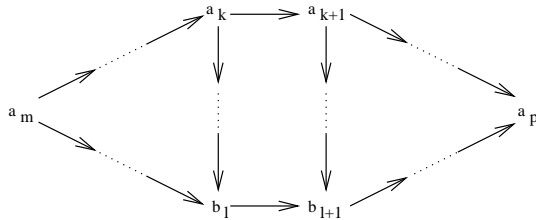


**Figure 19.** Diagram showing  $\tau_i : a_m \rightarrow a_p$  is well-defined.

between  $a_m$  and  $a_p$  compose to give the same natural isomorphism.

We define the adjacent transpositions between two objects  $a$  and  $b$  to be the arrows  $\tau_i = (i \ i + 1) : a \rightarrow b$  interchanging the leaf levels in positions  $i$  and  $i + 1$  that is given by any sequence of arrows between the objects  $a$  and  $b$  with only one terminal arrow. This definition is well-defined by the previous paragraph. Note that each adjacent transposition is a family of arrows index by source and target. We partition  $D$  into sections where each section is a sequence of arrows containing only one terminal arrow. Let  $a_0, \dots, a_r$  be the boundary vertices of these sections with  $a_{r+1} = a_0$ . Each sequence  $a_k \rightarrow \dots \rightarrow a_{k+1}$  of  $D$  corresponds to an adjacent transposition  $\tau_i : a_k \rightarrow a_{k+1}$ . We now show that the adjacent transpositions satisfy

$$\tau_i^2 = 1, \quad i = 1, \dots, n \tag{13}$$

$$\tau_i \tau_j = \tau_j \tau_i, \quad 1 \leq i < j - 1 \leq n - 1 \tag{14}$$

$$\tau_i \tau_{i+1} \tau_i = \tau_{i+1} \tau_i \tau_{i+1}, \quad i = 1, \dots, n - 2 \tag{15}$$

These are the generating relations for  $S_n$  from which it follows that  $D$  commutes.

Property (i): This follows because any sequence defining  $\tau_i : a \rightarrow b$  gives  $\tau_i : b \rightarrow a$  by inverting the sequence.

Property (ii): Given  $\tau_i : a \rightarrow c$ ,  $\tau_j : c \rightarrow b$ ,  $\tau_j : a \rightarrow d$  and  $\tau_i : d \rightarrow b$ . We construct sequences of internal arrows from  $a, b, c, d$  to vertices in  $(n - 3)$ -left reduced form as given by the diagram in figure 20. The branches shown are at the  $n - 1$  and  $n - 2$  levels



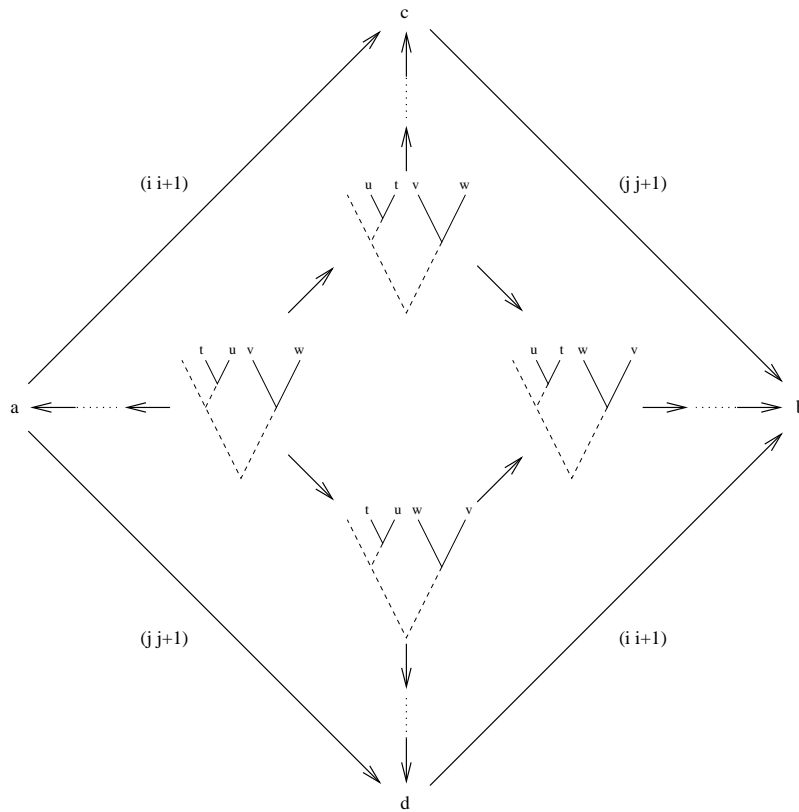


**Figure 20.** The property  $\tau_i \tau_j = \tau_j \tau_i$  whenever  $1 \leq i < j - 1 \leq n - 1$ .

and the terminates are in the  $i, i + 1, j, j + 1$  positions with their levels labelled  $t, u, v, w$ . The centre region is a natural square. All other regions commute because the definition of  $\tau_i, \tau_j$  is well-defined.

Property (iii): Given  $\tau_i : a \rightarrow c, \tau_{i+1} : c \rightarrow d, \tau_i : d \rightarrow b, \tau_{i+1} : a \rightarrow e, \tau_i : e \rightarrow f$  and  $\tau_{i+1} : f \rightarrow b$ ; we construct sequences of arrows as given by the diagram in figure 21. The central diagram is the Dodecagon diagram (figure 13) and commutes. The vertices of this diagram are taken to be in  $(n - 3)$ -left reduced form. The branches shown are at the  $n - 1$  and  $n - 2$  levels and the terminates are in the  $i, i + 1, i + 2$  positions with their levels labelled  $x, y, z$ . The sequences from  $a, b, c, d, e, f$  to the vertices of the centre region are taken to be composed only of internal arrows. Moreover, all the regions enclosed around the centre region commute because  $\tau_i, \tau_{i+1}$  are well-defined. This completes the proof of Theorem 2.

## 6. $\mathfrak{q}$ -Braided Pseudomonoidal Categories

The step from pseudomonoidal categories to  $\mathfrak{q}$ -pseudomonoidal categories was a natural one. Unfortunately one is faced with two fourteen vertex diagrams. Closer inspection of the diagram conditions shows that the  $\mathfrak{q}$ -Pentagon diagram concerns the action of  $\mathfrak{q}$  with branch terminates; the Dodecagon diagram concerns the action of  $\mathfrak{q}$  with leaf terminates; and the Quaddecagon and Dodecagon diagrams concern the action of  $\mathfrak{q}$  with mixed-

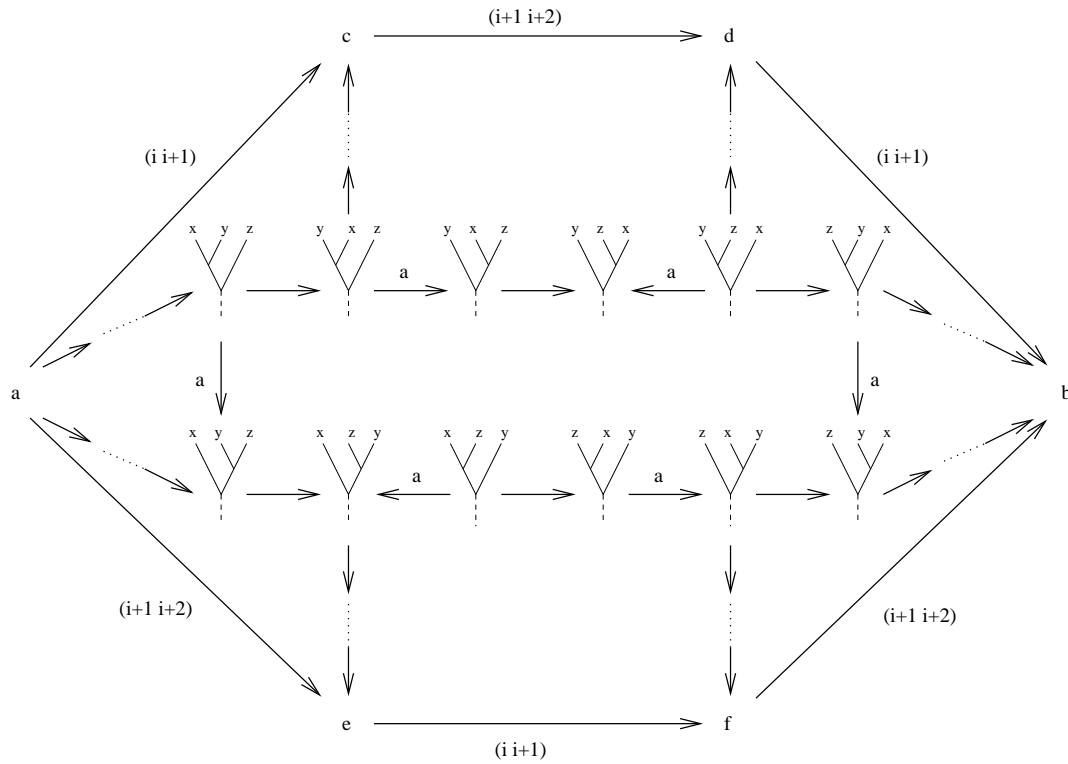


**Figure 21.** The property  $\tau_i \tau_{i+1} \tau_i = \tau_{i+1} \tau_i \tau_{i+1}$  whenever  $1 \leq i \leq n$ .

typed terminates. If we consider the full subcategory, **RRBTree** of reduced resolved binary trees, of **RBTree** then the two Quaddecagon diagrams are redundant. This leads to a coherence result that is weaker than  $\mathfrak{q}$ -pseudomonoidal coherence admitting a braid structure. The Dodecagon diagram is the Yang–Baxter equation for this braid. We begin by weakening our notion of  $\mathfrak{q}$ -premonoidal category.

**Definition 5** A  $\mathfrak{q}$ -braided pseudomonoidal category is a quadruple  $(\mathcal{C}, \otimes, \mathbf{a}, \mathfrak{q})$  where  $(\mathcal{C}, \otimes, \mathbf{a})$  is a pseudomonoidal category and  $\mathfrak{q} : \otimes \rightarrow \otimes$ , called the  $\mathfrak{q}$ -braid, is a natural automorphism satisfying the Dodecagon diagram (figure 10).

The  $\mathfrak{q}$  arising from the pseudomonoidal structure is in general different from the  $\mathfrak{q}$ -braid. The first is a natural automorphism for the functor  $\otimes(\otimes \times \otimes) : \mathcal{C}^4 \rightarrow \mathcal{C}$  corresponding to branch level interchange. The second is a natural automorphism for the functor  $\otimes : \mathcal{C}^2 \rightarrow \mathcal{C}$  corresponding to leaf level interchange. Every  $\mathfrak{q}$ -pseudomonoidal category is a  $\mathfrak{q}$ -braided strong pseudomonoidal category. For  $\mathfrak{q}$ -pseudomonoidal categories the  $\mathfrak{q}$  and  $\mathfrak{q}$ -braid are identified as the same natural automorphism.

We collect some results about **RRBTree**. A reduced RBTREE of length  $n$  is uniquely represented by an ordered pair of linear orderings. The first linear ordering of the numbers  $0, 1, \dots, n - 2$  represents the underlying IRB tree. The second linear ordering of the numbers  $1, 2, \dots, n$  is assigned to each leaf reading from left to right across the tree. The leaf level is given by adding  $n - 2$  to the number assigned by the second linear ordering. An example is given in figure 22. We call the first sequence (2310) the branch structure and the second sequence (14235) the leaf structure.

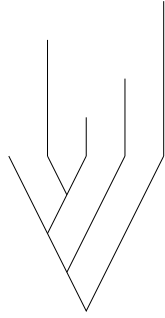


**Figure 22.** The reduced resolved binary tree (2310, 14235)

**Proposition 3**

- (i) For any two RRB trees of length  $n$  there is a finite sequence of primitive arrows transforming one into the other.
- (ii) Every RRB tree of length  $n$  is the source of at most  $n - 1$  distinct primitive arrows.
- (iii) There are  $n!(n - 1)!$  RRB trees of length  $n$ .

*Proof:* (i) Let  $B$  and  $B'$  be two RRB trees of length  $n$ . Every permutation is the product of a finite number of transpositions. Hence the result follows if very transposition of  $B$  to  $B'$  can be constructed from a sequence of primitive arrows. We construct (by Proposition 1) a sequence of internal arrows from  $B$  to an RRB tree with the  $i$  and  $i + 1$  terminates of the branch at level  $n - 1$ . Next we interchange  $i$  and  $i + 1$ . Finally we construct a sequence of internal arrows to  $B'$ .

(ii) We prove by induction on the length of the RRB tree. Suppose the result holds for RRB trees of length  $n$ . Given an RRB tree of length  $n + 1$  we consider the highest branch level to be a leaf. Then there are at most  $n - 1$  distinct primitive arrows. Including the highest branch we obtain an extra arrow for interchange and possibility an arrow for reattachment. The second arrow only occurs if the branch is joined to a pivot whose other terminate is a leaf. In this situation we over-counted an interchange of leaf levels. Hence there are at most  $n$  primitive operations.

(iii) There are  $(n - 1)!$  of arranging the branch structure and  $n!$  ways of rearranging the leaf structure.

The notion of RRB coherence follows directly from Theorem 2, part two of the proof. However, we can obtain a more general braided coherence result. We construct from **RRBTree** a braid category denoted **BRRBTree**. The objects are RRB trees. The arrows are reattachment and interchange of branches as for **RRBTree**. The  $q : \otimes \rightarrow \otimes$  natural automorphism corresponds to primitive arrows represented pictorially by the identification with a braid as given in figure 23. These arrows (or  $q$ -braids) act without regard for the level of the leaves. That is, there is no restriction that  $a > b$  for  $q$  and  $b < a$  for  $q^{-1}$ . The primitive  $q$ -braids are arrows that interchange two adjacent leaf levels provided the leaf levels interchanged are terminates of the same branch. The Dodecagon diagram arises from the  $q$ -Yang-Baxter diagram given in figure 24. There is a lot of freedom at the branch level. One way to avoid this is to choose an RRB tree

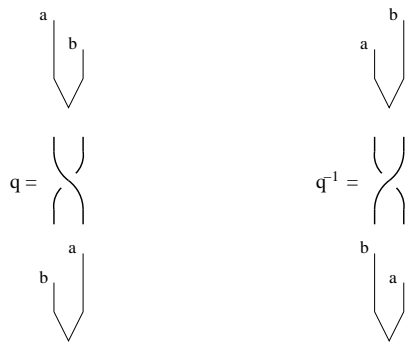


Figure 23. The  $q$ -braid primitive arrows.

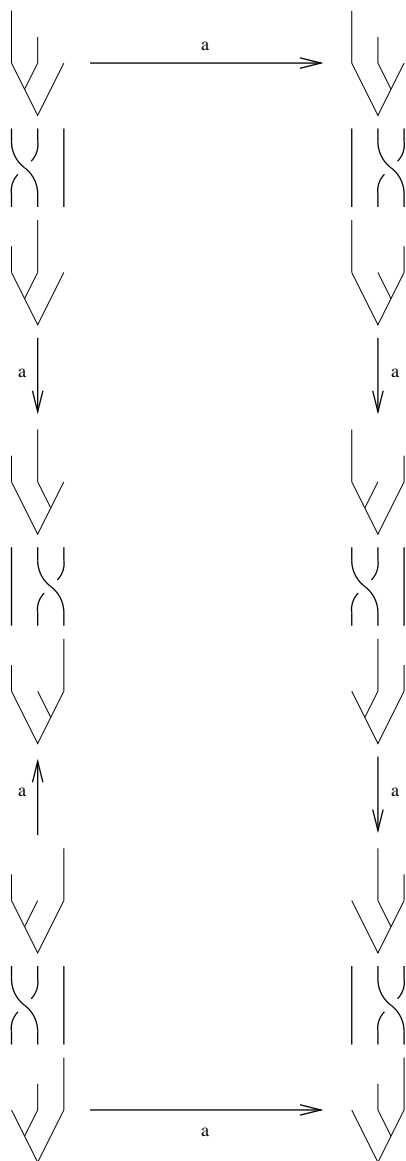


Figure 24. The  $q$ -Yang-Baxter diagram.

$a_n$  for each  $\mathbf{RRBTree}_n$  where  $\mathbf{RRBTree}_n$  is the full subcategory of  $\mathbf{RRBTree}$  containing all the RRB trees of length  $n$ . We call any set of objects  $(a_n)_{n \in \mathbb{N}}$  where  $a_n$  is of length  $n$  a frame for  $\mathbf{RRBTree}$ . Let  $\pi \in S_n$  and  $b_1 \dots b_n$  be the leaf structure for  $a_n$ . We define  $\pi a_n$  to be the RRB tree with the same branch structure as  $a_n$  and leaf structure  $b_{\pi(1)} \dots b_{\pi(n)}$  given by permuting the leaf structure of  $a_n$ . The primitive  $\mathfrak{q}$ -braids of length  $n$ , denoted  $\sigma_i$  where  $i = 1, \dots, n$ ; in the frame  $(a_n)_{n \in \mathbb{N}}$  are sequences of primitive arrows  $\sigma_i : a_n \rightarrow \dots \rightarrow (i \ i + 1)a_n$ , where  $1 \leq i \leq n$ . Moreover, these sequences can be any choice constructed using the rules of  $\mathbf{RRBTree}$ . The Dodecagon diagram implies the braid generating condition given in figure 25. The primitive  $\mathfrak{q}$ -braids generate the

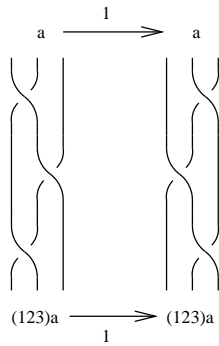


Figure 25. The braid generating condition.

Artin braid group. Under the functor **can** this  $\mathfrak{q}$ -braid group gives a braid coherence result. More generally we have the following coherence result.

**Theorem 3** *If  $\mathcal{C}$  is a category,  $\otimes : \mathcal{C} \times \mathcal{C} \rightarrow \mathcal{C}$  a bifunctor and  $\mathbf{a} : \otimes(\otimes \times 1) \rightarrow \otimes(1 \times \otimes)$  and  $\mathfrak{q} : \otimes \rightarrow \otimes$  natural isomorphisms then this structure is  $\mathfrak{q}$ -braided pseudomonoidal coherent if and only if the  $\mathfrak{q}$ -Pentagon diagram (figure 2), the  $\mathfrak{q}$ -Square diagrams (figure 6) and the Dodecagon diagram (figure 10) all commute.*

*Proof:* By part two of the proof of Theorem 2.

## 7. Unital Pseudomonoidal Categories

We now consider the issue of including an identity into pseudomonoidal and  $\mathfrak{q}$ -pseudomonoidal structures. This requires an identity object and natural isomorphisms for contracting the identity object on the left and right. The result is a unital pseudomonoidal or unital  $\mathfrak{q}$ -pseudomonoidal category. We only consider the pseudomonoidal case in what follows because the  $\mathfrak{q}$ -pseudomonoidal case follows similarly. The unital pseudomonoidal structure is monoidal when  $\mathfrak{q} = 1$ . Moreover, the coherent diagrams for a restricted premonoidal structure are monoidal whenever the identity object is involved. This is somewhat dissatisfying and will be resolved in the next section.

**Definition 6** *A unital pseudomonoidal category is a sextet  $(\mathcal{C}, \otimes, \mathbf{a}, \mathbf{l}, \mathbf{r}, e)$  such that  $(\mathcal{C}, \otimes, \mathbf{a})$  is a pseudomonoidal category (and hence allows construction of the natural*

automorphism  $\mathfrak{q}$ ),  $e$  is an object of  $\mathcal{C}$  called the identity object and  $\mathfrak{l} : e \otimes \_ \rightarrow 1$  and  $\mathfrak{r} : \_ \otimes e \rightarrow 1$  are natural isomorphisms satisfying the Triangle diagram (figure 26).

$$\begin{array}{ccc}
 (\alpha \otimes e) \otimes \beta & \xrightarrow{\mathfrak{a}_{\alpha,e,\beta}} & \alpha \otimes (e \otimes \beta) \\
 \searrow \mathfrak{r}_{\alpha} \otimes \mathfrak{l}_{\beta} & & \swarrow \mathfrak{l}_{\alpha} \otimes \mathfrak{l}_{\beta} \\
 & \alpha \otimes \beta &
 \end{array}$$

**Figure 26.** The Triangle diagram ( $T$ ).

$$\begin{array}{ccc}
 (e \otimes \alpha) \otimes \beta & \xrightarrow{\mathfrak{a}_{e,\alpha,\beta}} & e \otimes (\alpha \otimes \beta) \\
 \searrow \mathfrak{l}_{\alpha} \otimes \mathfrak{l}_{\beta} & & \swarrow \mathfrak{l}_{\alpha \otimes \beta} \\
 & \alpha \otimes \beta &
 \end{array}
 \quad
 \begin{array}{ccc}
 (\alpha \otimes \beta) \otimes e & \xrightarrow{\mathfrak{a}_{\alpha,\beta,e}} & \alpha \otimes (\beta \otimes e) \\
 \searrow \mathfrak{r}_{\alpha \otimes \beta} & & \swarrow \mathfrak{l}_{\alpha} \otimes \mathfrak{r}_{\beta} \\
 & \alpha \otimes \beta &
 \end{array}$$

**Figure 27.** The redundant Triangle diagrams ( $T_l$  and  $T_r$  respectively).

We assume for now that all the triangle diagrams hold (figures 26 and 27). We will shortly show that  $\mathfrak{q}$  is the identity whenever  $e$  is an index. Whence from the monoidal case only the Triangle diagram of figure 26 is required. The redundancy amongst the triangle diagrams was first pointed out by Kelly [14]. The  $\mathfrak{q}$  natural automorphism

$$\begin{array}{ccc}
 (e \otimes \alpha) \otimes (\beta \otimes \gamma) & \xrightarrow{\mathfrak{q}_{e,\alpha,\beta,\gamma}} & (e \otimes \alpha) \otimes (\beta \otimes \gamma) \\
 \searrow \mathfrak{l}_{\alpha} \otimes \mathfrak{l}_{\beta \otimes \gamma} & & \swarrow \mathfrak{l}_{\alpha} \otimes \mathfrak{l}_{\beta \otimes \gamma} \\
 & \alpha \otimes (\beta \otimes \gamma) &
 \end{array}
 \quad
 \begin{array}{ccc}
 (\alpha \otimes e) \otimes (\beta \otimes \gamma) & \xrightarrow{\mathfrak{q}_{\alpha,e,\beta,\gamma}} & (\alpha \otimes e) \otimes (\beta \otimes \gamma) \\
 \searrow \mathfrak{r}_{\alpha} \otimes \mathfrak{l}_{\beta \otimes \gamma} & & \swarrow \mathfrak{r}_{\alpha} \otimes \mathfrak{l}_{\alpha \otimes \gamma} \\
 & \alpha \otimes (\beta \otimes \gamma) &
 \end{array}$$

$$\begin{array}{ccc}
 (\alpha \otimes \beta) \otimes (e \otimes \gamma) & \xrightarrow{\mathfrak{q}_{\alpha,\beta,e,\gamma}} & (\alpha \otimes \beta) \otimes (e \otimes \gamma) \\
 \searrow \mathfrak{l}_{\alpha \otimes \beta} \otimes \mathfrak{l}_{\gamma} & & \swarrow \mathfrak{l}_{\alpha \otimes \beta} \otimes \mathfrak{l}_{\gamma} \\
 & (\alpha \otimes \beta) \otimes \gamma &
 \end{array}
 \quad
 \begin{array}{ccc}
 (\alpha \otimes \beta) \otimes (\gamma \otimes e) & \xrightarrow{\mathfrak{q}_{\alpha,\beta,\gamma,e}} & (\alpha \otimes \beta) \otimes (\gamma \otimes e) \\
 \searrow \mathfrak{l}_{\alpha \otimes \beta} \otimes \mathfrak{r}_{\gamma} & & \swarrow \mathfrak{l}_{\alpha \otimes \beta} \otimes \mathfrak{r}_{\gamma} \\
 & (\alpha \otimes \beta) \otimes \gamma &
 \end{array}$$

**Figure 28.** The triangle diagrams  $Q_1$ ,  $Q_2$ ,  $Q_3$  and  $Q_4$  satisfied by  $\mathfrak{q}$ .

satisfies the triangular diagrams of figure 28 because of the following lemma.

**Lemma 2** *Let  $\mathcal{C}$  be a category,  $\otimes : \mathcal{C} \times \mathcal{C} \rightarrow \mathcal{C}$  a bifunctor,  $e$  an object of  $\mathcal{C}$ ,  $\mathfrak{a}$ ,  $\mathfrak{q}$ ,  $\mathfrak{l}$  and  $\mathfrak{r}$  natural isomorphisms corresponding to associativity, deformation, left identity and right identity respectively. The following equivalences hold.*

- (i) If  $T_l$  commutes then the  $\mathfrak{q}$ -Pentagon diagram commutes if and only if  $Q_1$  commutes.
- (ii) If  $T_r$  commutes then the  $\mathfrak{q}$ -Pentagon diagram commutes if and only if  $Q_4$  commutes.
- (iii) If  $T$  commutes then the commutativity of any two of the  $\mathfrak{q}$ -Pentagon diagram,  $T_l$  and  $Q_2$  implies the third.
- (iv) If  $T$  commutes then the commutativity of any two of the  $\mathfrak{q}$ -Pentagon diagram,  $T_r$  and  $Q_3$  implies the third.

*Proof:* Each part follows by considering the  $\mathfrak{q}$ -Pentagon diagram with  $a = e$ ,  $d = e$ ,  $b = e$  and  $c = e$  respectively.

The bottom two arrows for each diagram in figure 26 compose to give an identity arrow. Hence we have the following proposition.

**Proposition 4** *Let  $(\mathcal{C}, \otimes, \mathbf{a}, \mathbf{l}, \mathbf{r}, e)$  be a unital pseudomonoidal category then  $\mathfrak{q}_{\alpha, \beta, \gamma, \delta} = 1_{(\alpha \otimes \beta) \otimes (\gamma \otimes \delta)}$  whenever any one of  $\alpha, \beta, \gamma, \delta$  is  $e$ .*

We move onto the issue of coherence. The coherence structure of interest is the category of internally resolved binary trees with nodules. A nodule is an open circle which may be attached to any leaf. Note that each nodule is uniquely determined by the adjacent internal node levels in the IRB tree number sequence. Whence a nodule is represented by placing a dot between these two levels. An example is given in figure 29. The length  $|B|$  of an IRB tree  $B$  with nodules is defined to be the number of leaves

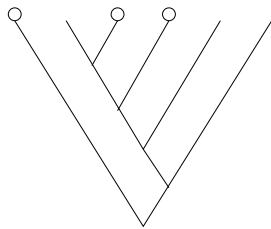


**Figure 29.** The IRB tree with nodules described by  $\cdot 04 \cdot 3 \cdot 21$ .

without nodules. The number of nodules is given by  $|\overline{B}| = \overline{B} - |B| + 1$ . The groupoid of IRB trees with nodules is denoted **IRNBTree**. The objects are IRB trees with nodules. The primitive arrows are inherited from **IRBTree** with the addition of primitive arrows for pruning and grafting nodules. The primitive arrows for the pruning of a nodule are given in figure 30. The dashed lines represent attachment sites to the remaining edges and nodes of the binary tree. Note that the source of the pruning arrow requires the level of a branch terminate to be on the next level up. The pruning arrow deletes a nodule from the tree and reduces by one the level of all nodes greater than the pivot level. The primitive arrows for grafting are given by the inverse of pruning. We have the following nodule version of Proposition 1.

**Proposition 5**

- (i) *Given two IRB trees with nodules of length  $n$  then there is a finite sequence of primitive arrows transforming one into the other.*

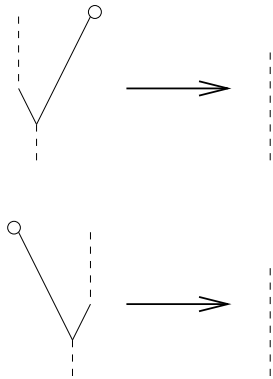


**Figure 30.** The primitive arrows for pruning nodules corresponding to iterates of left and right identity natural isomorphisms.

- (ii) Every IRB tree of height  $n$  with  $m$  nodules is the source of no more than  $5n - 1 + m$  distinct primitive arrows.
- (iii) There are  $\binom{n+1}{m} n!$  IRB trees of height  $n$  with  $m$  nodules.

*Proof:* (i) This follows from Proposition 1 since every IRB tree with nodules can have all of its nodules pruned and nodules may be grafted onto any edge.

(ii) We have that there are no more than  $n - 1$  **IRBTree** primitive arrows. There are  $m$  primitive arrows removing nodules and  $2|E|$  adding nodules since a nodule may be attached to either side of every edge. Finally the number of edges is  $|E| = 2n$  so summing the possibilities we obtain the result.

(iii) There are  $n!$  IRB trees of height  $n$  and for each such tree there are  $\binom{n+1}{m}$  ways of filling the  $n + 1$  leaves with  $m$  nodules.

The objects  $B$  of **IRNBTree** give rise to functors as in the nodule free situation with the following differences. The nodules stand in for the object  $e$ . If we let  $End_{\mathcal{C}}(e)$  denote the full subcategory of  $\mathcal{C}$  with the single object  $e$  then the functor  $\mathbf{can}(B) : End_{\mathcal{C}}(e)^{|B|} \times \mathcal{C}^{|B|} \rightarrow \mathcal{C}$  is given by contracting objects and arrows according to  $B$ . For example the tree of figure 27 gives a functor taking  $(c_1, c_2, c_3) \mapsto e \otimes (((c_1 \otimes e) \otimes e) \otimes c_2) \otimes c_3$  and  $(f_1, f_2, f_3, g_1, g_2, g_3) \mapsto f_1 \otimes (((g_1 \otimes f_2) \otimes f_3) \otimes g_2) \otimes g_3$  where  $c_i$  are objects in  $\mathcal{C}$ ,  $f_i$  are arrows in  $End_{\mathcal{C}}(e)$  and  $g_i$  are arrows in  $\mathcal{C}$ . We have the following expected coherence result.

**Theorem 4** *A pseudomonoidal category  $(\mathcal{C}, \otimes, \mathbf{a})$  with identity object  $e$  and natural isomorphisms  $\mathbf{l} : e \otimes \_ \rightarrow 1$  and  $\mathbf{r} : \_ \otimes e \rightarrow 1$  is unital pseudomonoidal coherent if and only if the Triangle diagram (figure 26) commutes.*

*Proof:* Let  $D$  be a diagram in  $\mathcal{D}(\mathbf{IRNBTree})$ . We define the rank of each vertex to be the number of nodules that it contains. The rank of  $D$  is defined to be the maximum of vertex ranks. Proof is by induction on diagram rank. The result holds for all diagrams of rank 0 by Theorem 1. Suppose the result is true for diagrams of rank  $n + 1$ . Let  $a_0, \dots, a_r$  be the vertices for some diagram  $D$  of rank  $n + 2$  given by reading around the outside. We identify  $a_{r+1}$  with  $a_0$ . We connect each vertex  $a_k$  of  $D$  to a vertex  $b_k$



obtained as follows: If  $a_k$  has rank  $n + 1$  then remove the left hand most nodule using the primitive arrow for its removal. If the rank of  $a_k$  is less than  $n + 2$  then define  $b_k = a_k$ . Connect  $b_k$  to  $b_{k+1}$  using a primitive arrow to form the square  $a_k a_{k+1} b_{k+1} b_k$ . This is checked by considering all possible cases. The squares obtained are natural or correspond to the triangle diagrams of figures 26, 27 and 28. Finally the diagram with vertices  $b_0, \dots, b_r$  constructed is of rank less than or equal to  $n$  and by the induction hypothesis commutes. Hence the diagram  $D$  commutes.

### 8. Symmetric $\mathfrak{q}$ -Pseudomonoidal Categories

We now weave a natural isomorphism for commutativity into the picture. We consider a commutativity natural isomorphism that is symmetric. Moreover, additional symmetric natural isomorphisms can be constructed from  $\mathfrak{c}$  and  $\mathfrak{q}$ . The weakening of a symmetric  $\mathfrak{q}$ -pseudomonoidal structure to a symmetric  $\mathfrak{q}$ -braided pseudomonoidal structure is an obvious step. The  $\mathfrak{q}$ -braid is symmetric. It is only this latter structure that admits what should properly be called a symmetric  $\mathfrak{q}$ -monoidal category.

Define the flip functor to be  $\tau : \mathcal{C} \times \mathcal{C} \rightarrow \mathcal{C} \times \mathcal{C}$  where  $(a, b) \mapsto (b, a)$ .

**Definition 7** A symmetric  $\mathfrak{q}$ -pseudomonoidal category is a pentuple  $(\mathcal{C}, \otimes, \mathfrak{a}, \mathfrak{q}, \mathfrak{c})$  where  $(\mathcal{C}, \otimes, \mathfrak{a}, \mathfrak{q})$  is a  $\mathfrak{q}$ -pseudomonoidal category,  $\mathfrak{c} : \otimes \rightarrow \otimes \tau$  is a natural isomorphism such that  $\mathfrak{c}$  and  $\mathfrak{q}$  are symmetric and the Square diagram (figure 31), the Hexagon diagram (figure 32) and the Decagon diagrams (figures 33 and 34) all commute.

$$\begin{array}{ccc}
 \alpha \otimes \beta & \xrightarrow{\mathfrak{c}_{\alpha, \beta}} & \beta \otimes \alpha \\
 \mathfrak{q}_{\alpha, \beta} \downarrow & & \uparrow \mathfrak{q}_{\beta, \alpha} \\
 \alpha \otimes \beta & \xleftarrow{\mathfrak{c}_{\beta, \alpha}} & \beta \otimes \alpha
 \end{array}$$

**Figure 31.** The Square diagram.

The underlying binary tree groupoid is the groupoid of numbered RB trees denoted **NRBTree**. The objects are RB trees (abbreviated NRB trees) of any length  $n$  with each leaf assigned a distinct number from  $\{1, \dots, n\}$ . These numbers we write above the leaf levels in the level sequence for the underlying RB tree. An example is given in figure 35. The primitive arrows are inherited from **RBTree** together with additional primitive arrows corresponding to  $\mathfrak{c}$  defined as follows. Let  $B$  be an NRB tree. For any internal node  $p$  let  $m < p$  be the first internal node to the left of  $p$  and  $n < p$  the first internal node to the right of  $p$ ; we can interchange the subsequences between  $m$  and  $p$  and  $p$  and  $n$ . Pictorially this corresponds to swaping the two subtrees rooted at the terminates of the pivot  $p$ . Since  $\mathfrak{c}$  is symmtric the levels of the terminates is irrelevant. The objects of **NRBTree** induce functors as in the **RBTree** situation with the difference that the objects have been permuted according to the numbers on the leaves. If  $a_1, \dots, a_n$  is the

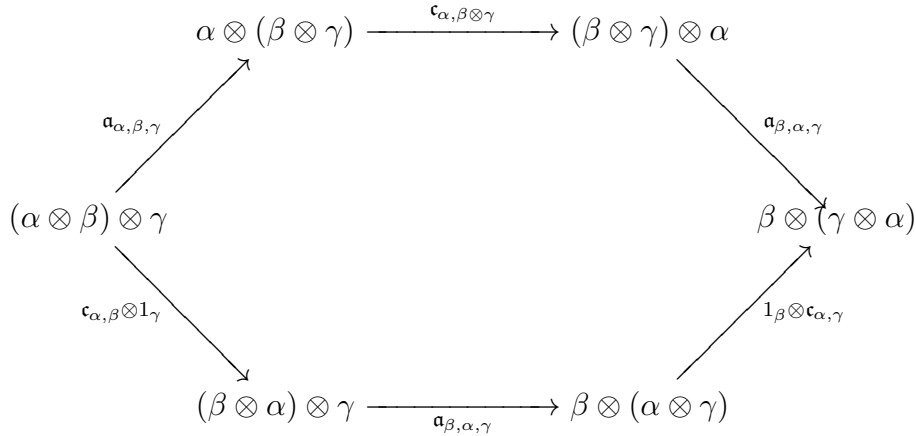


**Figure 32.** The Hexagon diagram.

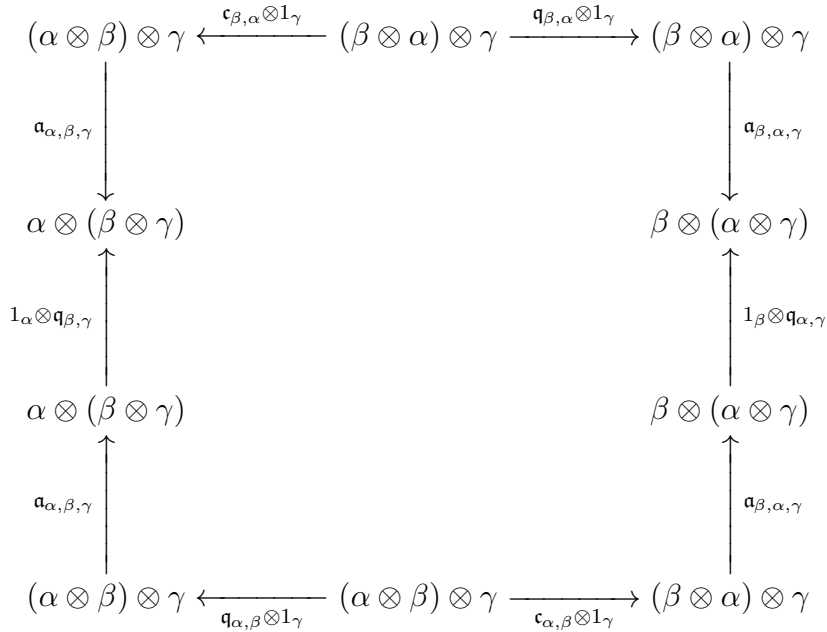


**Figure 33.** The First Decagon diagram.

sequence of leaf numbers then the permutation is given by  $(1, \dots, n) \mapsto (a_1, \dots, a_n)$ . The Square diagram and the Hexagon diagram originate from those diagrams in **NRBTree** given in figures 36 and 37 respectively. Note that the Hexagon diagram is independent of the terminate levels. The diagram of figure 37 is one out of  $3!$  diagrams of length three. This is why  $\mathfrak{c}$  must be commutative or in other words indifferent to the levels of the terminates. Furthermore, because of the Square diagram the natural isomorphisms  $\mathfrak{c}\mathfrak{q} : \otimes \rightarrow \otimes\tau$  and  $\mathfrak{q}\mathfrak{c} : \otimes \rightarrow \otimes\tau$  are equal, symmetric and correspond to binary tree operations that swap terminates without interchanging levels.

The groupoid **NRBTree** has the properties of the following Proposition.

**Proposition 6**

- (i) Given two NRB trees of length  $n$  then there is a finite sequence of primitive arrows transforming one into the other.

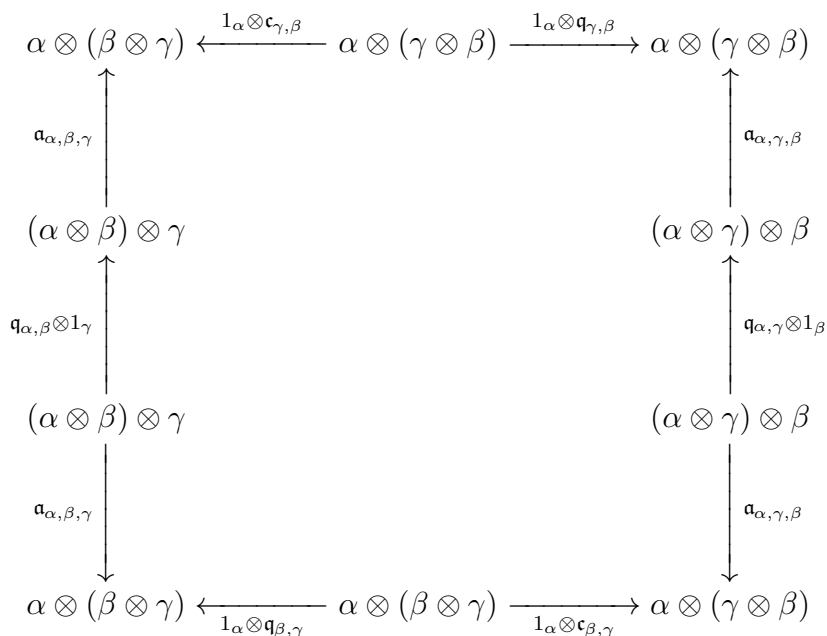


Figure 34. The Second Decagon diagram.

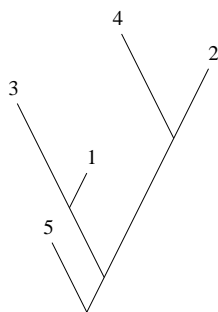


Figure 35. The NRB tree given by  $\begin{matrix} 5 & 3 & 1 & 4 & 2 \\ 206341857 \end{matrix}$ .

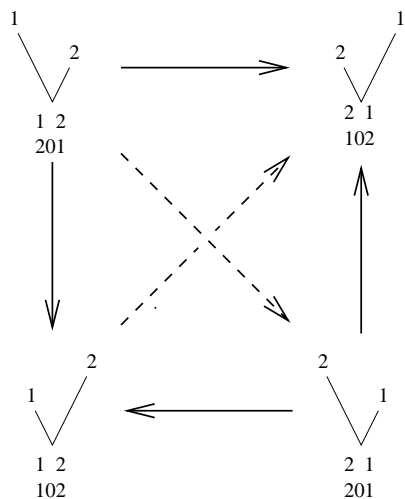
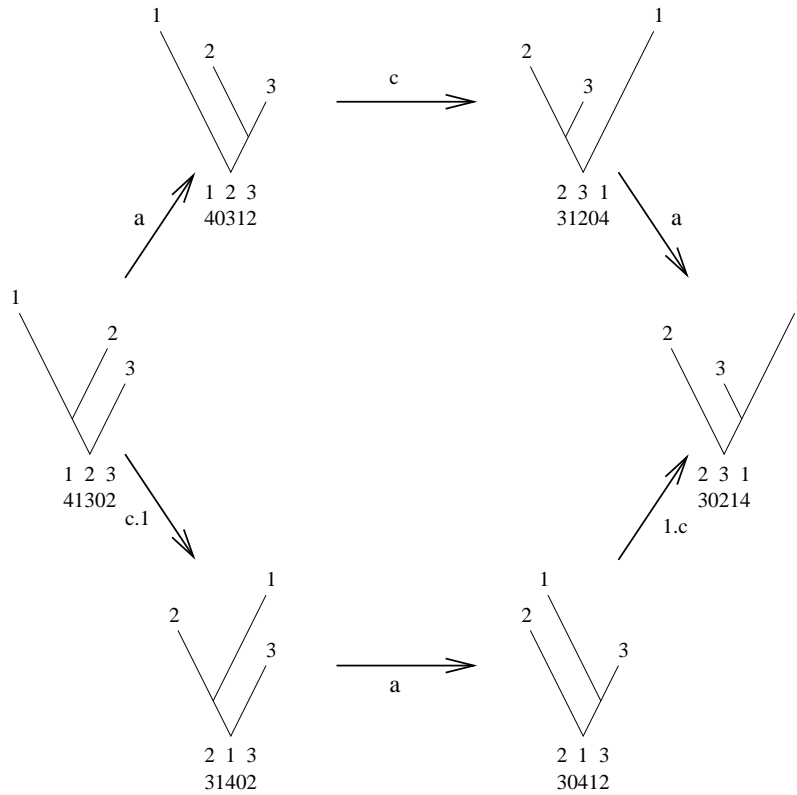


Figure 36. Diagram in NRBTree underlying the Square diagram.



**Figure 37.** Diagram in **NRBTree** underlying the Hexagon diagram.

- (ii) Every NRB tree of length  $n$  is the source of at most  $3(n - 1)$  distinct primitive arrows.
- (iii) Let  $T(n)$  denote the number of RB trees of length  $n$ . The number of NRB trees of length  $n$  is  $n!T(n)$ .

*Proof:* (i) Let  $B$  and  $B'$  be two NRB trees of length  $n$ . Every permutation is the product of a finite number of transpositions. Hence the result follows if every transposition of  $B$  to  $B'$  can be constructed from a sequence of primitive arrows. We construct (by Proposition 2) a sequence of internal arrows from  $B$  to an NRB tree with the  $i$  and  $i + 1$  terminates of the branch at level  $n - 1$ . Next we swap the terminates. Finally we construct a sequence of internal arrows to  $B'$  (again by Proposition 2).

(ii) There are a maximum of  $2(n - 1)$  possible distinct primitive RB arrows. Every internal node admits a primitive arrow corresponding to a swap. There are  $n - 1$  internal nodes.

(iii) There are  $T(n)$  choices of RB trees. Each can be numbered in  $n!$  ways.

The final step is the coherence result.

**Theorem 5** A  $\mathfrak{q}$ -pseudomonoidal category  $(\mathcal{C}, \otimes, \mathfrak{a}, \mathfrak{q})$  where  $\mathfrak{q}$  is symmetric and  $\mathfrak{c} : \otimes \rightarrow \otimes\tau$  is a symmetric natural isomorphism for commutativity is symmetric  $\mathfrak{q}$ -pseudomonoidal coherent if and only if the Square diagram (figure 31) and the Hexagon diagram (figure 32) and two Decagon diagrams (figures 33 and 34) all commute.

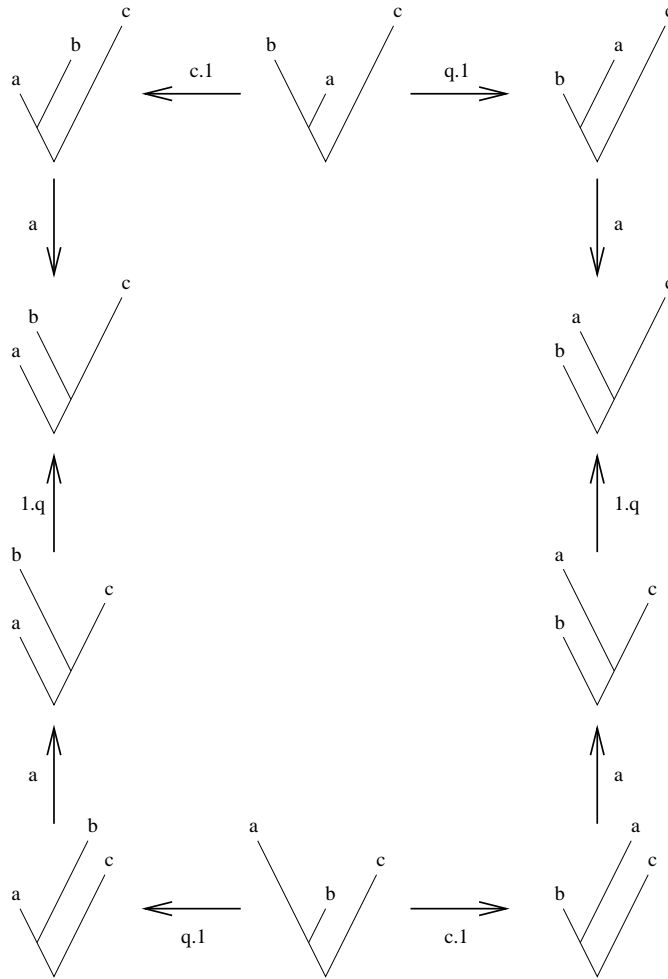


**Figure 38.** Diagram in  $\mathbf{NRBTree}$  underlying the First Decagon diagram.

*Proof:* We first show that every iterate of  $\mathbf{c}$  can be replaced by a sequence of iterates of  $\mathbf{q}$ ,  $\mathbf{a}$  and those  $\mathbf{c}$  corresponding to transposition of adjacent leaves. Consider an arrow  $a \rightarrow b$  that is an iterate of  $\mathbf{c}$ . We define its rank  $n$  to be the minimum number of adjacency transpositions required to generate the permutation. We inductively reduce to the desired sequence. If  $n = 2$  then we have our desired sequence. Otherwise  $n > 2$  and we let  $p$  be the pivot point in  $a$  (and hence in  $b$ ) for the arrow  $a \rightarrow b$ . Let  $k, l$  be the terminates of  $p$ . At least one of  $k, l$  is an internal node. Suppose it is  $k$ . If  $k > l$  then we replace the arrow using the Square diagram. Now we have  $k < l$ . We use the Hexagon diagram to replace  $\text{It}_p(\mathbf{c})$  with a sequence of five arrows where the only iterates of  $\mathbf{c}$  are  $\text{It}_p(\mathbf{c}.1)$  and  $\text{It}_p(\mathbf{c})$ . These iterates have rank strictly less than  $n$ . Continuing this procedure inductively we eventually replace  $a \rightarrow b$  with a sequence of arrows containing  $2^n$  adjacent transpositions. These transpositions are the only iterates of commutativity.

The second step of the proof is to show that two alternative sequences of arrows, each containing exactly one adjacent transposition (iterate of  $\mathbf{c}$ ) between objects encloses a region that commutes. Let two such sequences be  $a_1 \rightarrow \cdots \rightarrow a_r$  with adjacent transposition  $\text{It}_k(\mathbf{c}) : a_i \rightarrow a_{i+1}$  pivoting about  $k$  with terminate levels  $a, b$ ; and

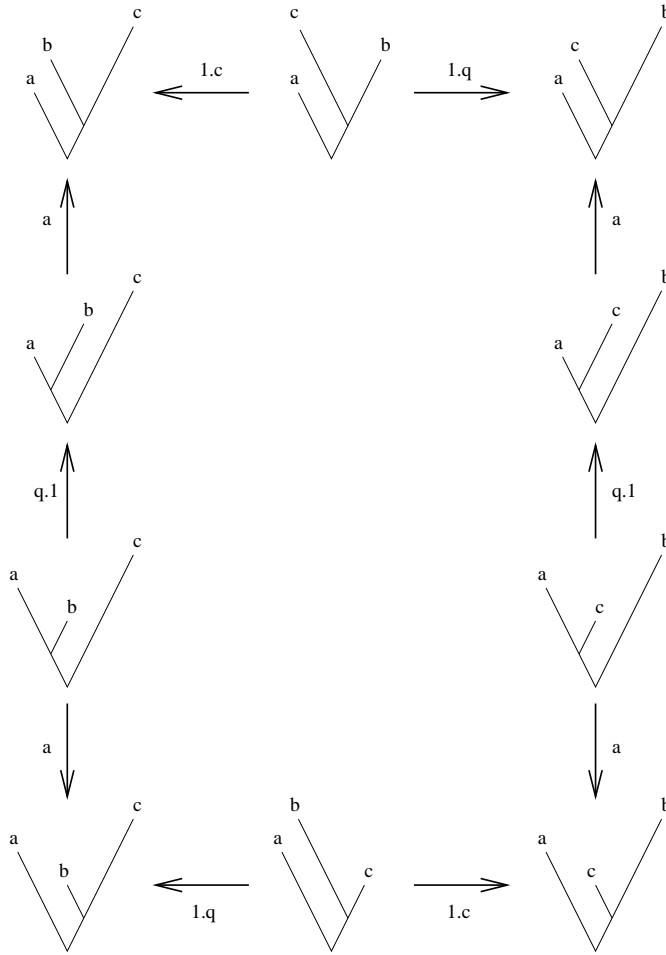


**Figure 39.** Diagram in **NRBTree** underlying the Second Decagon diagram.

$b_1 \rightarrow \dots \rightarrow b_s$  with adjacent transposition  $It_l(\mathbf{c}) : b_{i'} \rightarrow b_{i'+1}$  pivoting about  $l$  with terminate levels  $c, d$ . Also  $a_1 = b_1$  and  $a_r = b_s$ . We assume that  $k > l$ ,  $c$  is to the left of  $a$  and  $d$  is to the right of  $b$ . The other seven possibilities follow similarly. A construction demonstrating the region enclosed commutes is given in figure 40. The sequence of arrows around the top is  $a_1 \rightarrow \dots \rightarrow a_r$ . The sequence around the bottom is  $b_1 \rightarrow \dots \rightarrow b_s$ . Each vertical arrow stands in for a sequence of arrows to keep the size of the diagram acceptable. Starting from the top we proceed to describe the ladder of regions. The sides of the top region are identical and each arrow keeps  $a, b$  and  $k$  fixed. This region commutes by naturality and Theorem 2. The next region down is the Square diagram. The next down has identical sides composed of arrows keeping  $a, b$  and  $l$  fixed. This commutes by Theorem 2 and naturality. The next region down is the first Decagon diagram. The next region down has identical sides composed of arrows keeping  $a, d$  and  $l$  fixed. This region commutes by Theorem 2 and naturality. The next region down is the second Decagon diagram. The final region at the base has identical sides composed of arrows keeping  $c, d$  and  $l$  fixed. This region commutes by Theorem 2 and naturality. The two side regions commute by Theorem 2.

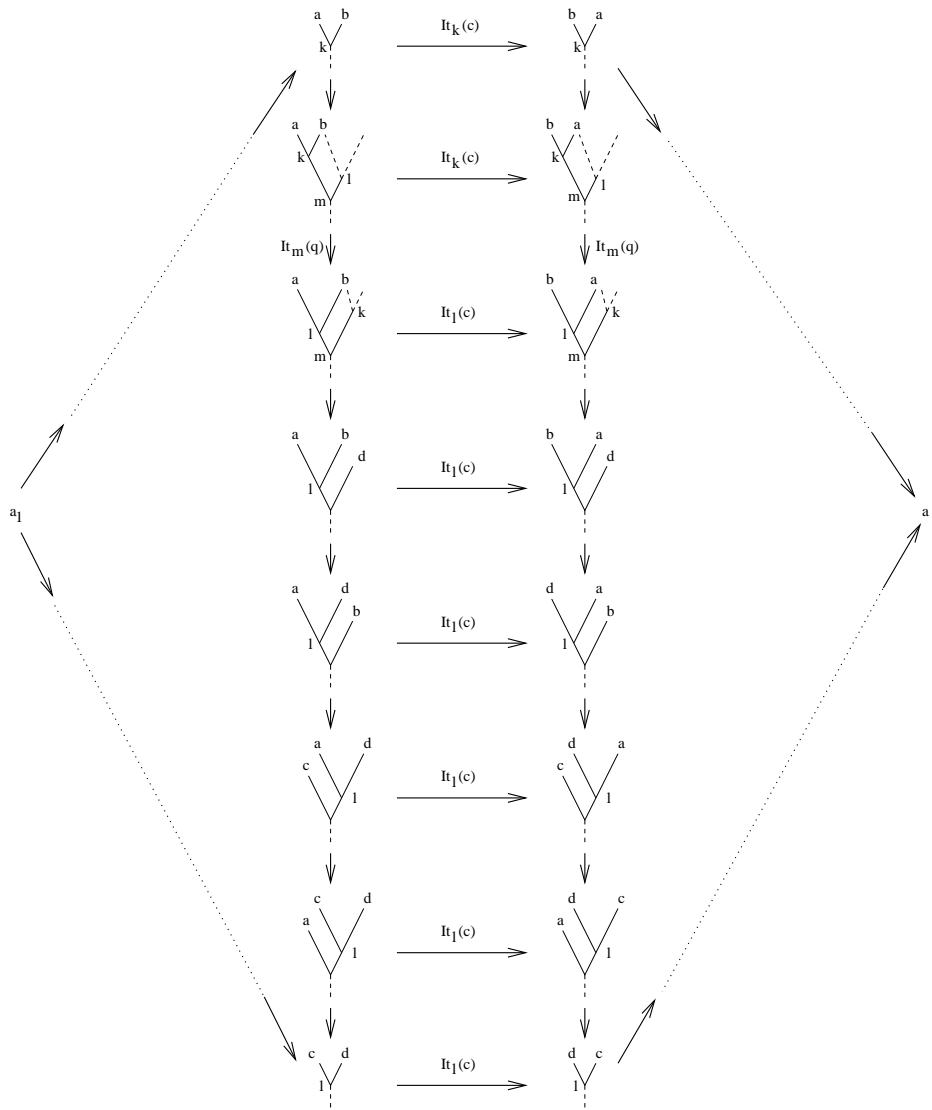


**Figure 40.** The equivalence of two adjacent position transposing sequences.

The final step is to show that any diagram  $D$  of rank  $n+1$  commutes. This proceeds in a similar way to the proof of Theorem 2 part two. We replace every iterate of  $\mathbf{c}$  with a sequence containing only iterates of  $\mathbf{c}$  that are adjacent transpositions. We define the adjacent transpositions between two objects  $a$  and  $b$  to be the arrows  $\tau_i = (i \ i+1) : a \rightarrow b$  swapping positions  $i$  and  $i+1$  given by any sequence of arrows between the objects  $a$  and  $b$  with only one terminal arrow. This definition is well-defined by the previous paragraph. Note that the adjacent transpositions are families of arrows index by source and target. We partition  $D$  into sections where each section is a sequence of arrows containing only one terminal arrow. Let  $a_0, \dots, a_r$  be the boundary vertices of these sections with  $a_{r+1} = a_0$ . Each sequence  $a_k \rightarrow \dots \rightarrow a_{k+1}$  corresponds to an adjacent transposition  $\tau_i : a_k \rightarrow a_{k+1}$ . We now show that the adjacent transpositions satisfy the generating relations of the permutation group  $S_{n+1}$ .

$$\tau_i^2 = 1, \quad i = 1, \dots, n \tag{16}$$

$$\tau_i \tau_j = \tau_j \tau_i, \quad 1 \leq i < j \leq n \quad (17)$$

$$\tau_i \tau_{i+1} \tau_i = \tau_{i+1} \tau_i \tau_{i+1}, \quad i = 1, \dots, n - 1 \quad (18)$$

Properties (i), (ii) and (iii) are proved by an obvious modification to the verification in the proof of Theorem 2 part two. For property (iii) we note that the Dodecagon diagram embedded in figure 21 is replaced by the diagram of figure 41. The middle region is a

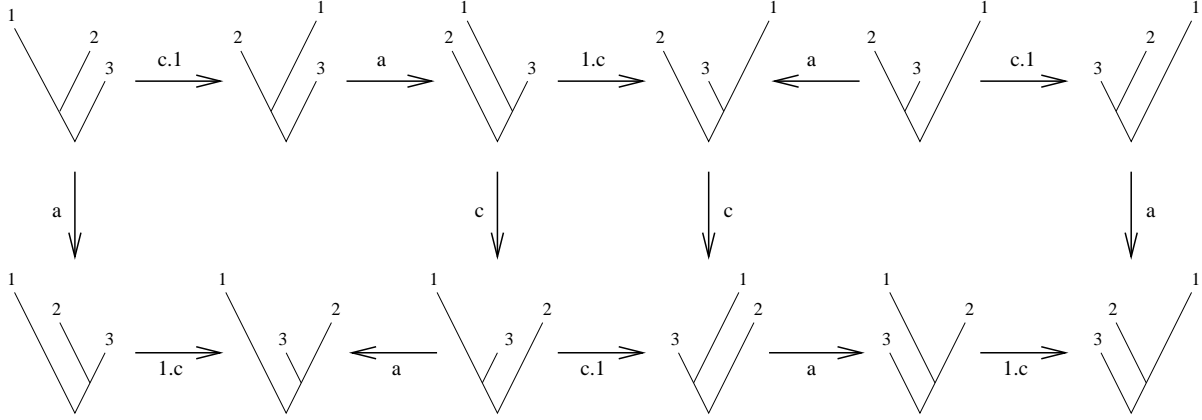


**Figure 41.** Verification of the property  $\tau_i \tau_{i+1} \tau_i = \tau_{i+1} \tau_i \tau_{i+1}$ .

naturality square and the two side regions are Hexagon diagrams. This completes the proof.

Symmetric Pseudomonoidal coherence follows as a corollary to Theorem 5. We give the definition leaving the details to the reader.

**Definition 8** *A symmetric pseudomonoidal category is a quadruple  $(\mathcal{C}, \otimes, \mathbf{a}, \mathbf{c})$  where  $(\mathcal{C}, \otimes, \mathbf{a})$  is a pseudomonoidal category,  $\mathbf{q}$  and  $\mathbf{c}$  are symmetric, the Square diagram, Hexagon diagram and Decagon diagrams (extended to branch points) hold and the diagrams of figure 42 hold.*

### 9. Symmetric $\mathbf{q}$ -Monoidal Categories

The difficulty with unital pseudomonoidal structures is that the notion of identity is handled monoidally. This rather defeats the underlying motivation for considering pseudomonoidal categories in the first place. Including the notion of identity has proven to be a delicate balance. A pseudomonoidal category is too general to incorporate this notion. On the other hand the  $\mathbf{q}$ -pseudomonoidal category has too many conditions resulting in the severe conditions that  $\mathbf{q}$  is symmetry,  $\mathbf{q}_{\alpha, \beta} \otimes 1_\gamma = \mathbf{q}_{\alpha \otimes \beta, \gamma}$  and  $1_\alpha \otimes \mathbf{q}_{\beta, \gamma} = \mathbf{q}_{\alpha, \beta \otimes \gamma}$  for all objects  $\alpha, \beta, \gamma$ . Moreover, these conditions are not represented by any binary tree diagram in the coherence groupoid. The right level of structure is that of a  $\mathbf{q}$ -braided premonoidal category. Well not quite. The existence of a commutativity natural isomorphism is also required. In the absence of commutativity one is faced with requiring an infinite number of diagrams to hold in order to guarantee coherence.



$$\begin{array}{ccc}
 (\alpha \otimes \beta) \otimes (\gamma \otimes \delta) & \xrightarrow{c_{\alpha,\beta} \otimes 1_{\gamma \otimes \delta}} & (\beta \otimes \alpha) \otimes (\gamma \otimes \delta) \\
 \downarrow \mathfrak{q}_{\alpha,\beta,\gamma,\delta} & & \downarrow \mathfrak{q}_{\beta,\alpha,\gamma,\delta} \\
 (\alpha \otimes \beta) \otimes (\gamma \otimes \delta) & \xrightarrow{c_{\alpha,\beta} \otimes 1_{\gamma \otimes \delta}} & (\beta \otimes \alpha) \otimes (\gamma \otimes \delta) \\
 \\ 
 (\alpha \otimes \beta) \otimes (\gamma \otimes \delta) & \xrightarrow{1_{\alpha \otimes \beta} \otimes c_{\gamma,\delta}} & (\alpha \otimes \beta) \otimes (\delta \otimes \gamma) \\
 \downarrow \mathfrak{q}_{\alpha,\beta,\gamma,\delta} & & \downarrow \mathfrak{q}_{\alpha,\beta,\delta,\gamma} \\
 (\alpha \otimes \beta) \otimes (\gamma \otimes \delta) & \xrightarrow{1_{\alpha \otimes \beta} \otimes c_{\gamma,\delta}} & (\alpha \otimes \beta) \otimes (\delta \otimes \gamma)
 \end{array}$$

**Figure 42.** Additional square diagrams required for symmetric pseudomonoidal coherence.

**Definition 9** A symmetric  $\mathfrak{q}$ -monoidal category is an octuple  $(\mathcal{C}, \otimes, \mathfrak{a}, \mathfrak{q}, \mathfrak{c}, \mathfrak{l}, \mathfrak{r}, e)$  where  $(\mathcal{C}, \otimes, \mathfrak{a}, \mathfrak{q})$  is a  $\mathfrak{q}$ -braided pseudomonoidal category,  $(\mathcal{C}, \otimes, \mathfrak{a}, \mathfrak{c})$  is a symmetric pseudomonoidal category,  $e$  is an object of  $\mathcal{C}$  called the identity and  $\mathfrak{l} : e \otimes \_ \rightarrow 1$  and  $\mathfrak{r} : \_ \otimes e \rightarrow 1$  are natural isomorphisms satisfying the small and large  $\mathfrak{q}$ -Triangle diagrams (figures 43 and 44)

$$\begin{array}{ccccccc}
 (\alpha.e).\beta & \xrightarrow{\mathfrak{a}_{\alpha,e,\beta}} & \alpha.(e.\beta) & \xleftarrow{1_{\alpha} \cdot \mathfrak{q}_{e,\beta}} & \alpha.(e.\beta) & \xleftarrow{\mathfrak{a}_{\alpha,e,\beta}} & (\alpha.e).\beta & \xleftarrow{\mathfrak{q}_{\alpha,e} \cdot 1_{\beta}} & (\alpha.e).\beta & \xrightarrow{\mathfrak{a}_{\alpha,e,\beta}} & \alpha.(e.\beta) \\
 \downarrow \mathfrak{r}_{\alpha} \cdot 1_{\beta} & & & & & & & & & & \downarrow 1_{\alpha} \cdot \mathfrak{l}_{\beta} \\
 \alpha.\beta & \xleftarrow{\mathfrak{q}_{\alpha,\beta}} & \alpha.\beta & & \alpha.\beta & & \alpha.\beta & & \alpha.\beta & & \alpha.\beta
 \end{array}$$

**Figure 43.** The Large  $\mathfrak{q}$ -Triangle diagram.

The  $\mathfrak{q}$ -Triangle diagrams collapse to the Triangle diagrams (of monoidal categories) when  $\mathfrak{q} = 1$ . There are no  $\mathfrak{q}$ -Triangle diagrams corresponding to the redundant triangle diagrams that were originally in the definition of a monoidal category. The redundancy amongst the original Triangle diagrams was pointed out by Kelly [14].

The underlying binary tree category is the groupoid of numbered RRB trees with nodules, denoted **NRRNBTree**. As we did earlier we represent a nodule by attaching a small circle to the leaf. An RRB tree with nodules is represented by an ordered pair of linear orderings. The first entry gives the branch structure. The second entry the leaf structure. Leaves with nodules are represented by placing a line under its level. The length of an RRB tree with nodules is the number of leaves less the number of nodules.

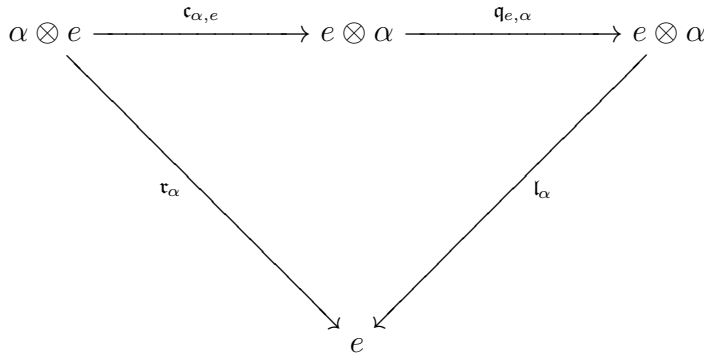


Figure 44. The Small  $q$ -Triangle diagram.

These trees under the **can** functor give functors where the nodules stand in for the identity. A numbered RRB tree of length  $n$  attaches a number  $1, \dots, n$  uniquely to each of the nodule free leaves.

The arrows of **NRRTree** are generated by the primitive arrows inherited from **NRBTree** together with primitive arrows corresponding to left and right identity that we now define. Given an RRB tree  $B$  with nodules having  $n$  leaves; we can prune a nodule at level  $n + 1$  that is the left terminate of a branch at level  $n - 1$  whose right terminate leaf is at level  $n$ . This leaves the leaf at level  $n$ . All other leaf levels are lowered by two. We can prune a nodule at level  $n$  that is the right terminate of a branch at level  $n - 1$  whose left terminate leaf is at level  $n + 1$ . This leaves the leaf at level  $n$ . All other leaf levels are lowered by two. The grafting arrows are given by the converse of the pruning operation described. These primitive arrows are given in figure 45. The diagrams in **RRNBTree** underlying the  $q$ -Triangle diagrams are given

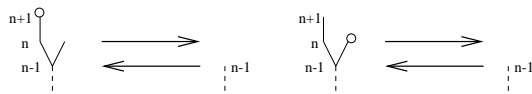


Figure 45. The pruning and grafting primitive arrows of **RRNBTree**.

by figures 46 and 47.

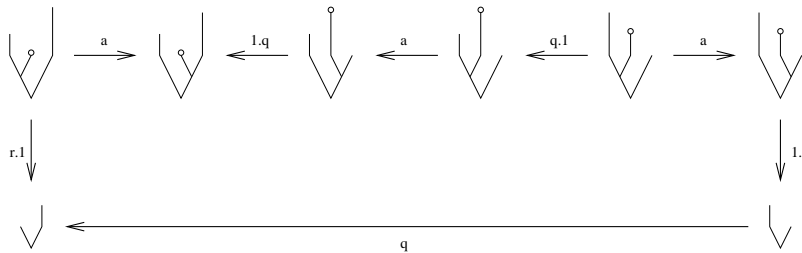
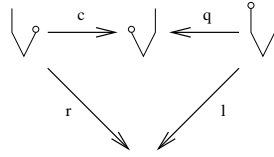


Figure 46. Diagram in **NRRTree** underlying the Large  $q$ -Triangle diagram.

**Proposition 7**



**Figure 47.** Diagram in **NRRNBTree** underlying the Small  $\mathfrak{q}$ -Triangle diagram.

- (i) Given two numbered *RRB* trees with nodules of length  $n$  then there is a finite sequence of primitive arrows transforming one into the other.
- (ii) Every numbered *RRB* tree with  $m$  nodules of length  $n$  is the source of at most  $2(n + m)$  distinct primitive arrows.
- (iii) The number of *RRB* trees with  $m$  nodules of length  $n$  is  $2(n + m)!(n + m - 1)n!$ .

*Proof:* (i) Let  $B$  and  $B'$  be any two numbered *RRB* trees with nodules of length  $n$ . Choosing each nodule of  $B$  in turn we can rearrange using a sequence of **NRBTree** primitive arrows so that it is a terminate of the highest branch and this branch's terminates are on the next two levels up. Clearly we can prune the nodule. Applying the same procedure to  $B'$  we can construct a similar sequence of primitive arrows. Clearly  $B$  and  $B'$  are connected by a sequence of primitive arrows (Proposition 3).

(ii) There are at most  $n + m - 1$  **RRBTree** primitive arrows. The only possibilities for pruning or grafting is when the highest branch has a terminate at the lowest level. There are at most two possibilities in this situation. Finally every branch, of which there are  $n + m - 1$ , admits a reflection.

(iii) There are  $(n + m)1(n + m - 1)!$  *RRB* trees of length  $n + m$ . There are  $n!$  ways of numbering the nodule free leafs. Nodules may only be grafted to the leaf at level  $n + m$ . There are precise two ways of doing this.

Now that we have a groupoid of binary trees describing the diagrams of a symmetric  $\mathfrak{q}$ -monoidal category we formulate the notion of coherence in the by now standard way.

**Theorem 6** *A symmetric  $\mathfrak{q}$ -braided pseudomonoidal category  $(\mathcal{C}, \otimes, \mathfrak{a}, \mathfrak{q}, \mathfrak{c})$  with an object  $e$  and natural isomorphisms  $\mathfrak{l} : e \otimes \_ \rightarrow 1$  and  $\mathfrak{r} : \_ \otimes e \rightarrow 1$  is symmetric  $\mathfrak{q}$ -monoidal coherent if and only if the  $\mathfrak{q}$ -Triangle diagrams (figures 43 and 44) both commute.*

*Proof:* The proof is by induction. Define the rank of a vertex to be the number of leafs and the rank of a diagram to be the maximum of its vertex ranks. The theorem holds for rank 3 diagrams. Suppose all diagrams with rank  $n$  are coherent. Let  $D$  be a diagram of rank  $n + 1$  with vertices  $a_0, a_1, \dots, a_r$  reading around the outside and put  $a_{r+1} = a_0$ . If every vertex of  $D$  has rank  $n + 1$  then there are no primitive arrows pruning/grafting nodules. Hence  $D$  commutes by Theorem 5. Otherwise we divide  $D$  into maximal sequences where all the vertices have rank  $n + 1$  alternating with none of the vertices have rank  $n + 1$ . Let one such sequence be where all the vertices have rank  $n + 1$  be  $a_k \rightarrow \dots \rightarrow a_l$ . The arrows  $a_{k-1} \rightarrow a_k, a_l \rightarrow a_{l+1}$  fall into three cases.

**Case (a):** The arrows do not prune/graft a nodule into the first or second position.

If both arrows are of this type then we substitute the sequence  $a_{k-1} \rightarrow \cdots \rightarrow a_{l+1}$  according to figure 48. The top horizontal line is the sequence  $a_{k-1} \rightarrow \cdots \rightarrow a_{l+1}$ .

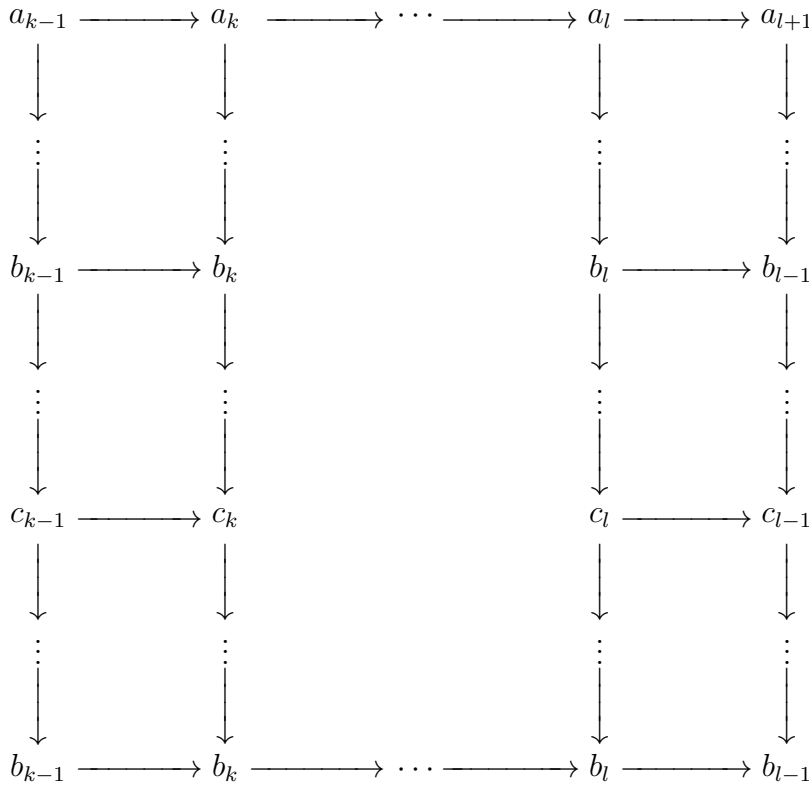


**Figure 48.** Removal of vertices with rank  $n + 1$  from  $D$ .

Suppose that the highest leaf level is to the left of the nodule being grafted by the arrow  $a_{k-1} \rightarrow a_k$  and that this arrow corresponds to an iterate of the right identity. We construct identical sequences of **RRBTree** arrows from  $a_{k-1}$  to  $b_{k-1}$  and from  $a_k$  to  $b_k$ . The arrow  $b_{k-1} \rightarrow b_k$  is an iterate of  $\tau$  and the region enclosed commutes by naturality. The vertices  $b_{k-1}$  and  $b_k$  are of the form given in figure 49. The top left hand region in

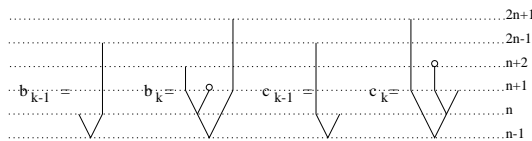


**Figure 49.** The vertices  $b_{k-1}$ ,  $b_k$ ,  $c_{k-1}$  and  $c_k$ .

figure 48 commutes by naturality and Theorem 5. The next region down is taken to be the large  $q$ -Triangle diagram where the vertices  $c_{k-1}$  and  $c_k$  are as given in figure 49. We construct identical sequences of **RRBTree** arrows from  $c_{k-1}$  to  $d_{k-1}$  and from  $c_k$  to  $d_k$ . The arrow  $d_{k-1} \rightarrow d_k$  is an iterate of  $\tau$  where the vertices  $d_{k-1}$  and  $d_k$  are of the form given in figure 50. The region these sequences (in figure 48) enclose commutes. If the arrow  $a_{k-1} \rightarrow a_k$  was an iterate of the left identity then the above construction follows similarly with the middle left hand region of figure 48 being a combination of the

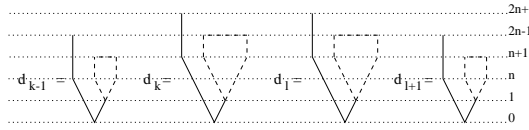


Figure 50. The vertices  $d_{k-1}$ ,  $d_k$ ,  $d_l$  and  $d_{l+1}$ .

small and large  $\mathfrak{q}$ -Triangle diagrams. The only other possibility for  $a_{k-1} \rightarrow a_k$  is if the highest leaf level is to the right of the nodule being grafted. In this case the construction proceeds directly from  $a_{k-1}$  to  $d_{k-1}$  and from  $a_k$  to  $d_k$ .

The left hand side vertical sequences of arrows in figure 46 is constructed as for the right hand side with all the enclosed regions commuting. Finally we connect  $d_k$  to  $d_l$  using a sequence of **NRBTree** arrows that do not pivot about the root. The region enclosed contains no arrows for grafting nor pruning nodules and by Theorem 5 commutes. The sequence running around the bottom of the diagram from  $a_{k-1}$  to  $d_{k-1}$  to  $d_{l+1}$  to  $a_{l+1}$  is substituted for the maximal sequence.

**Case (b):** The arrows do not prune/graft a nodule into the first position but at least one of these does into the second position. Suppose  $a_{k-1} \rightarrow a_k$  grafts a nodule into the second position. This arrow is one of the top horizontal arrows given in the diagrams of figure 51. If it is the first diagram then we see that the small  $\mathfrak{q}$ -Triangle diagram allows

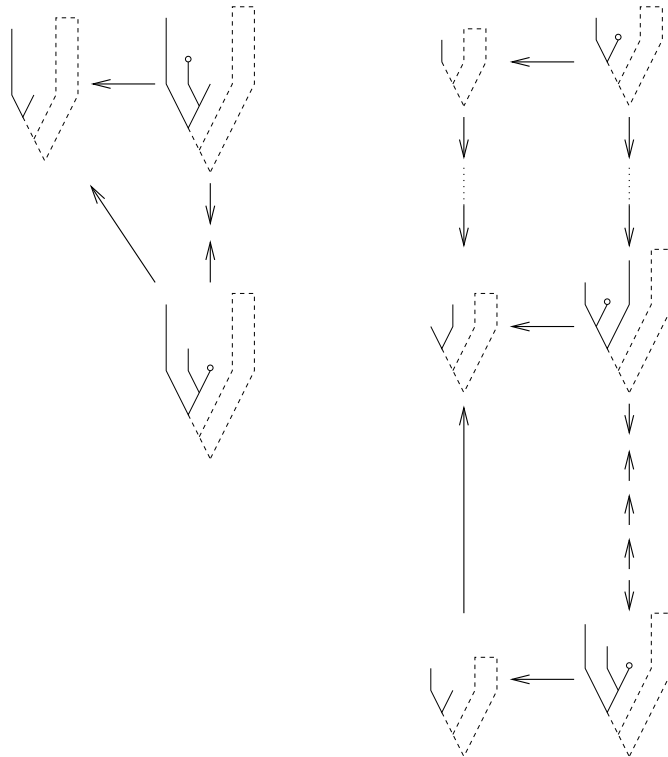


Figure 51. Diagrams used to reduce from case (b) to case (a).

us to substitute it for a sequence grafting a nodule into the third position. If it is the second diagram then we construct the two sides of the top region using two identical

sequences of **RRBTree** arrows that do not pivot about the highest branch and maintain the first and second positions as terminates. As before the region enclosed commutes. Finally the bottom region is the large  $\mathfrak{q}$ -Triangle diagram. We use the sequence running around the bottom of the diagram (of figure 51) to substitute for  $a_{k-1} \rightarrow a_k$  for which the primitive arrow for grafting a nodule into the third position. We apply a similar substitution to  $a_l \rightarrow a_{l+1}$  if it prunes a nodule from the second position. The new maximal sequence falls into case (b).

**Case (c):** At least one arrow prunes/grafts a nodule into the first position. We replace all arrows grafting/pruning a nodule into the first with one grafting/pruning into the second position using the small  $\mathfrak{q}$ -Triangle diagram. The new maximal sequence falls into case (a) or (b).

We divide  $D$  up into maximal sequences as before. Let  $a_k \rightarrow \dots \rightarrow a_l$  and  $a_{k'} \rightarrow \dots \rightarrow a_{l'}$  be consecutive maximal sequences. The vertices  $a_{k-1}, \dots, a_{l+1}, a_{k'-1}, \dots, a_{l'+1}$  all have the highest leaf as the left terminate of the root. We replace the joining sequence  $a_{l+1} \rightarrow \dots \rightarrow a_{k'-1}$  by an alternative sequence of **NRBTree** primitive arrows with the highest leaf as the left terminate of the root. The region enclosed commutes by Theorem 5. Conituning this substitution inductively we construct a diagram where every vertex has the left terminate of the root as the highest leaf. Moreover, this diagram commutes if and only if  $D$  commutes. Hence by the induction hypothesis  $D$  commutes. This completes the proof.

### 10. Summary

The prototype of all structures considered in this paper is that of a pre-monoidal/pseudomonoidal category. This gave rise to the notion of a  $\mathfrak{q}$  natural automorphism which in the coherence groupoid corresponds to interchanging the level of two branch points. Extending this to include leaves leads to the notion of  $\mathfrak{q}$ -pseudomonoidal category. Prohibiting the interchange of a leaf level with a branch level leads to the notion of a  $\mathfrak{q}$ -braided pseudomonoidal category. The hierarchy of these structures is given in table 3 together with their coherence groupoid. Each structure admits restricted and

structure	coherence groupoid
pseudomonoidal	<b>IRBTree</b>
$\mathfrak{q}$ -braided pseudomonoidal	<b>RRBTree</b>
$\mathfrak{q}$ -pseudomonoidal	<b>RBTree</b>
monoidal	<b>BTree</b>

**Table 3.** Coherence groupoids underlying natural associativity structures.

symmetric versions. Only the symmetric  $\mathfrak{q}$ -symmetric pseudomonoidal category admits a  $\mathfrak{q}$ -monoidal structure which we call symmetric  $\mathfrak{q}$ -monoidal. The relationship between all the structures studied in this paper is depicted in figure 52. Finally further work on

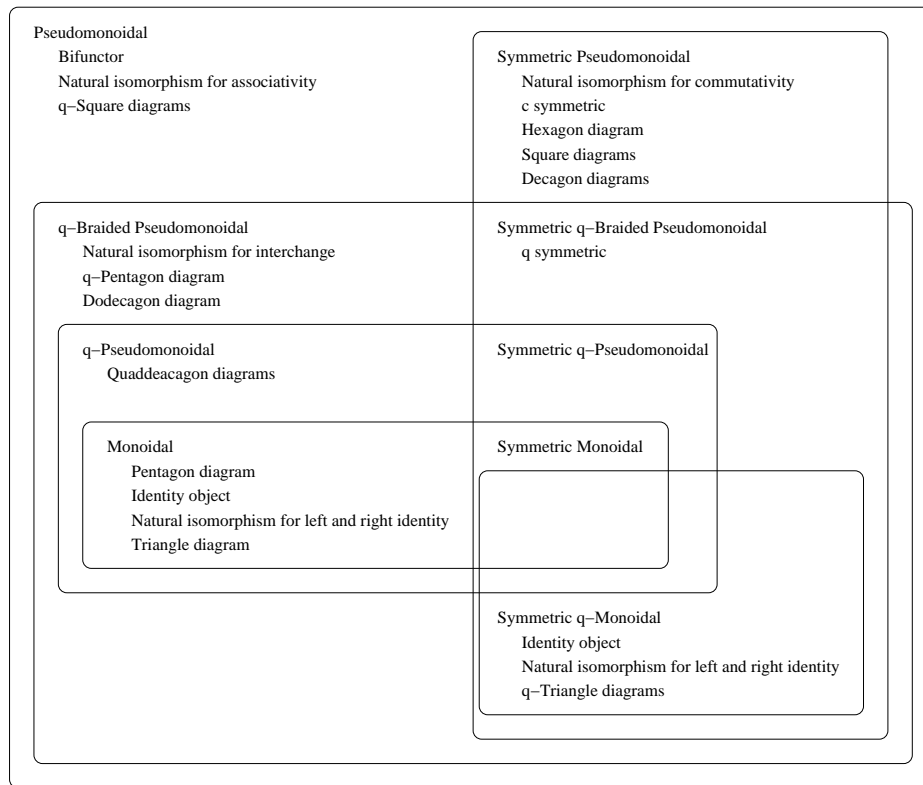
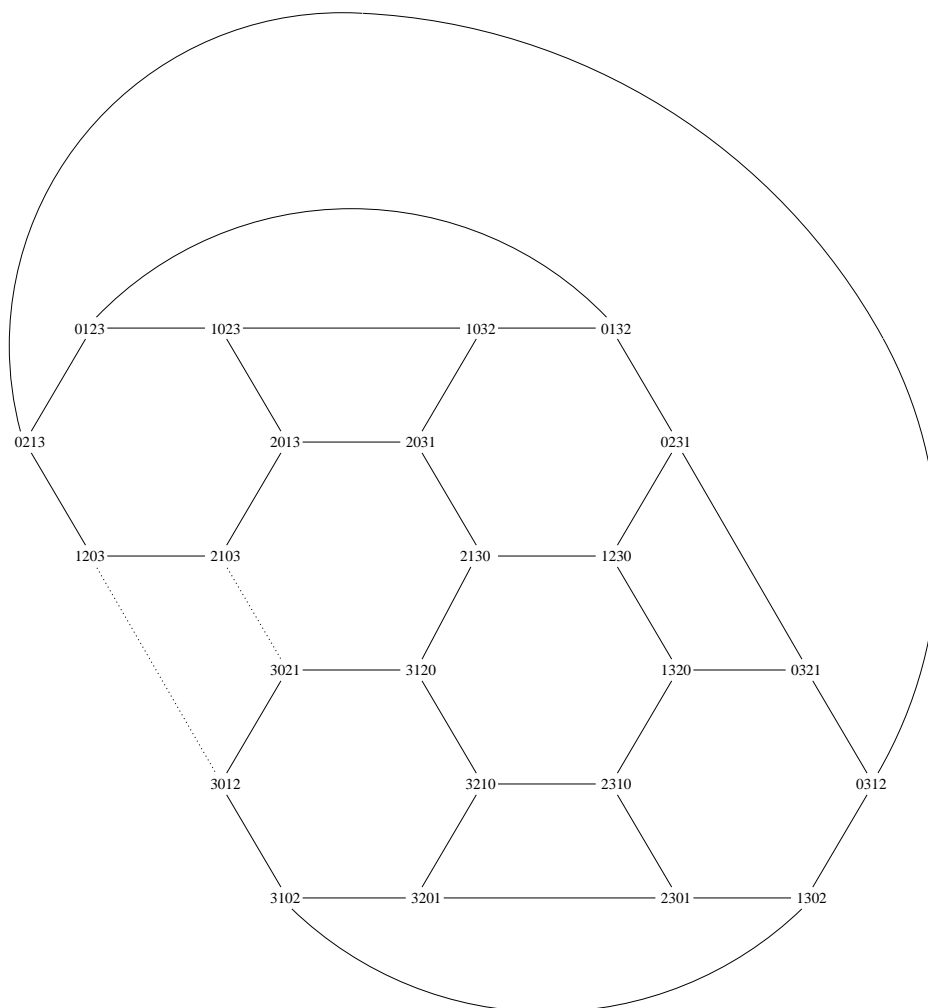


Figure 52. Overview of pseudomonoidal structures.

braided premonoidal coherence and the breaking of unital structure is soon to appear [22].

### Appendix A

A  $q$ -pseudomonoidal category allows one to ponder the existence of a  $q$ -associahedra as a deformation of the associahedra for monoidal categories. The  $q$ -associahedron for words of length four is the  $q$ -Pentagon diagram. For words of length five it is the planar diagram given in figure 53. Note that the dotted lines represent disallowed primitive operations for level interchange. The hexagons correspond to the  $q$ -diagram and the quadrilaterals are natural squares. Hence the twelve vertex diagram around the perimeter commutes. However, the diagram does not fold into a polyhedron. The diagram wraps around a truncated polyhedron as given by figure 54. The missing strip corresponds to the twelve vertex diagram encircling figure 53. This partially formed polyhedron is not what one would like to take as the  $q$ -associahedron. Instead we utilise the connection with permutations described in section 4. The  $q$ -associahedron is replaced by a permutahedron. The edges do not correspond to primitive arrows. They are, however, constructed from primitive arrows and correspond to adjacent transpositions.



**Figure 53.** The primitive arrows for words of length five.

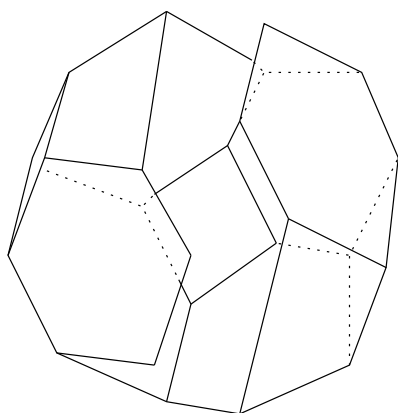


**Figure 54.** Folding of the planar diagram of figure 51.

### Acknowledgements

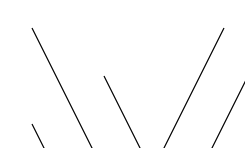
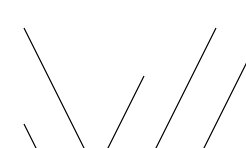
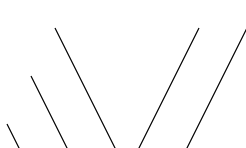
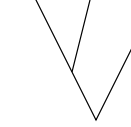
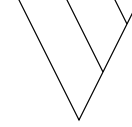
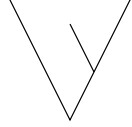
The author wishes to thank Prof. Ross Street for supporting this research at Macquarie University, Division of Communication and Information Sciences, N.S.W.

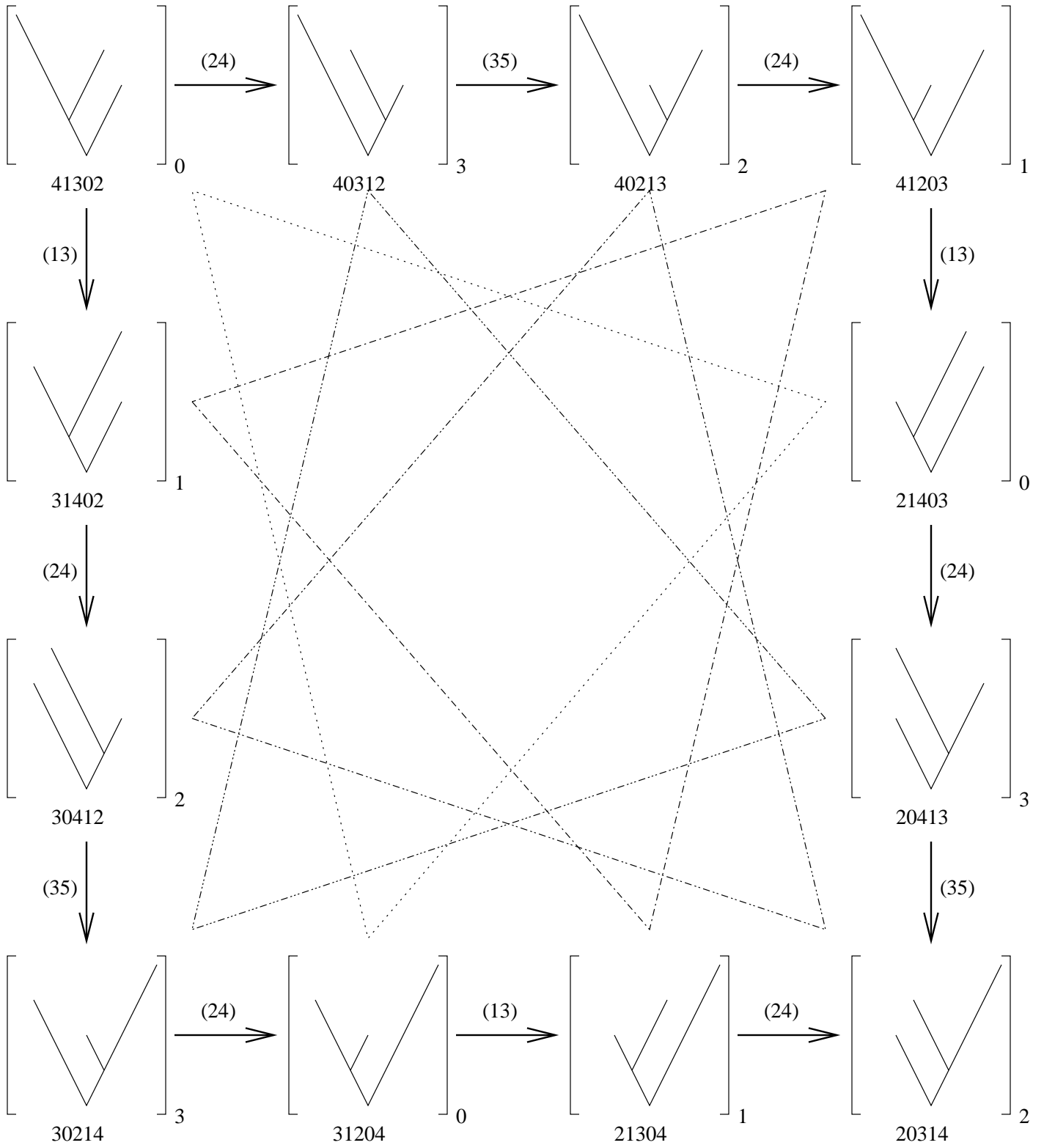


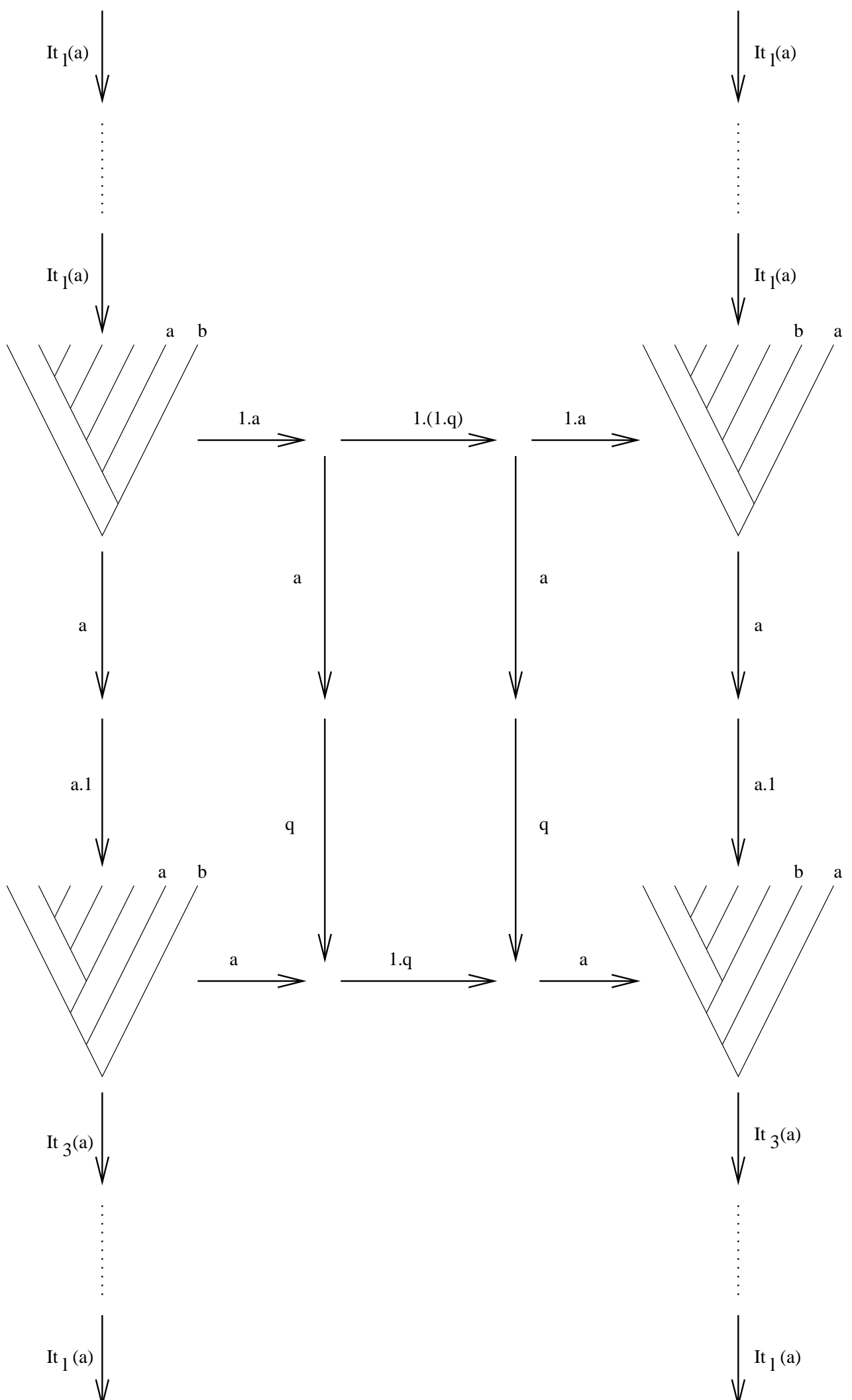
2109, Australia. I would like to acknowledge Daniel Steffen and Dr. Mark Weber for pointing out the links between  $T(n)$ , tangent numbers and up/down permutations. Also I thank Dr. Michael Batanin for some useful discussions, and Prof. Jim Stasheff for useful suggestions on an early draft.

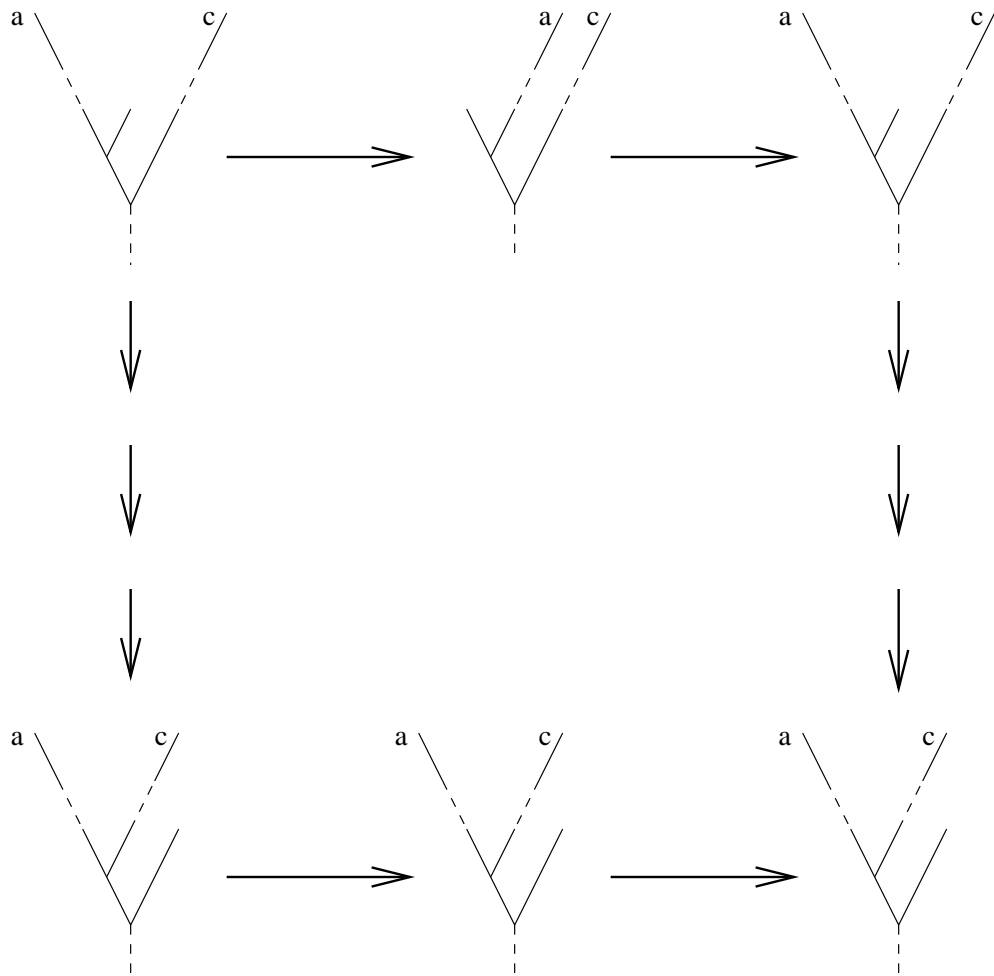
## References

- [1] W. P. Joyce, *Vertex Calculus in Premonoidal Categories: I. The Racah–Wigner Calculus and Natural Statistics*, submitted to Rev. Math. Phys. (2003)
- [2] W. P. Joyce, *Vertex Calculus in Premonoidal Categories: II. Coupling and the Clebsch–Gordon Vertex*, submitted to Rev. Math. Phys. (2003)
- [3] W. P. Joyce, *Vertex Calculus in Premonoidal Categories: III. Recoupling and Recoupling Coefficients*, submitted to Rev. Math. Phys. (2003)
- [4] W. P. Joyce, *Vertex Calculus in Premonoidal Categories: IV. The Wigner Symbols*, preprint University of Canterbury (2003)
- [5] W. P. Joyce, *Vertex Calculus in Premonoidal Categories: V. Many–particle Quantum Theory and Scattering*, preprint University of Canterbury (2003)
- [6] W. P. Joyce, *The Boson/Fermion Statistic for  $SU(3)$  Colour requires Quark confinement* to appear in Proceedings of the XXIV International Colloquium on Group Theoretical Methods in Physics, Paris (2002)
- [7] W. P. Joyce, *Diagram Projection in the Racah–Wigner Category*, J. Math. Phys. **42**, 1346–1363 (2001)
- [8] J. Bénabou, *Categories avec multiplication*, C. R. Acad. Sci. Paris Sér. I Math. **256** 1887–1890 (1963)
- [9] S. Mac Lane, *Natural Associativity and Commutativity*, Rice University Studies **49** 28–46 (1963)
- [10] S. Mac Lane, *Categories for the Working Mathematician*, Springer–Verlag N.Y. (1971)
- [11] C. Kassel, *Quantum Groups*, Springer–Verlag N.Y. (1995)
- [12] W. P. Joyce, P. H. Butler and H. J. Ross, *The Racah–Wigner Category*, to appear in Can. J. Phys. (2002)
- [13] W. P. Joyce, *Formulation of the Racah–Wigner Calculus using Category Theory*, Ph.D. thesis University of Canterbury (2000)
- [14] G. M. Kelly, *On Mac Lanes Coherence for Natural Associativities*, J. Alg. **1** pp397–402 (1964)
- [15] J. D. Stasheff, *Homotopy associativity of  $H$ –spaces, I*, Trans. Am. Math. Soc. **108**, 275–292 (1963)
- [16] G. M. Kelly, *Coherence theorems for lax algebras and distributive laws*, Lecture Notes in Maths **420** Springer–Verlag Berlin and New York pp281–375 (1974)
- [17] M. L. Laplaza, *Coherence for Distributivity*, Lecture notes in Maths **281** Springer–Verlag Berlin and New York 29–65 (1972)
- [18] A. Joyal and R. Street, *Braid Tensor Categories*, Adv. Math. **102** 20–78 (1993)
- [19] N. S. Yanofsky, *Obstructions to Coherence: Natural Noncoherent Associativity*, J. Pure Appl. Alg. **147**, 175–213 (2000)
- [20] A. Tonks, *Relating the associahedron and the permutahedron*, Contemporary Math. **202**, 33–36 (1997)
- [21] J. Millar, N. J. A. Sloane and N. E. Young, *A new Operation on Sequences: the Boustrophedon Transform*, J. Comb. Theory A **76** 44–54 (1996)
- [22] W. P. Joyce *Braided Premonoidal Coherence* submitted to J. Pure Appl. Alg. (2003)

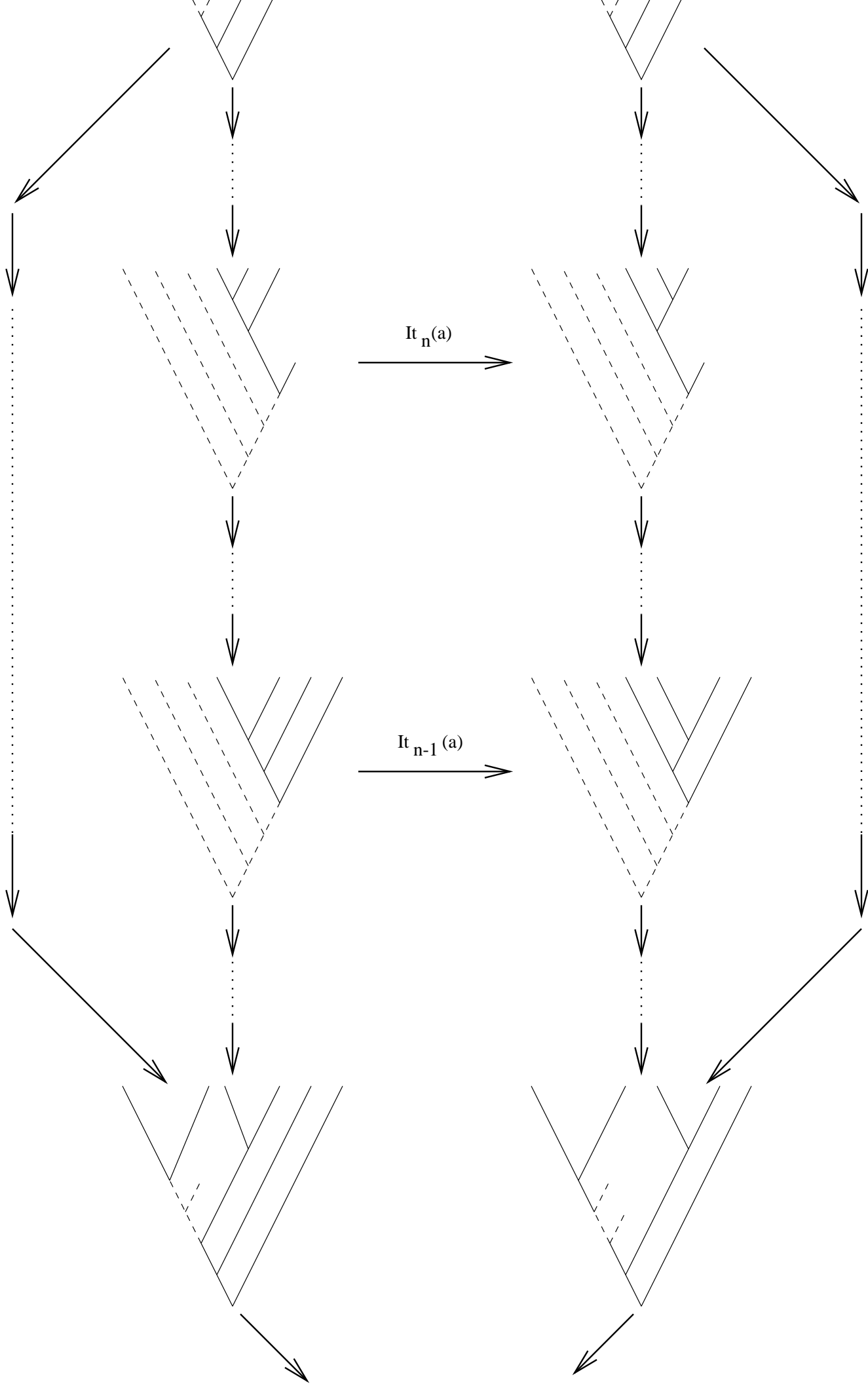


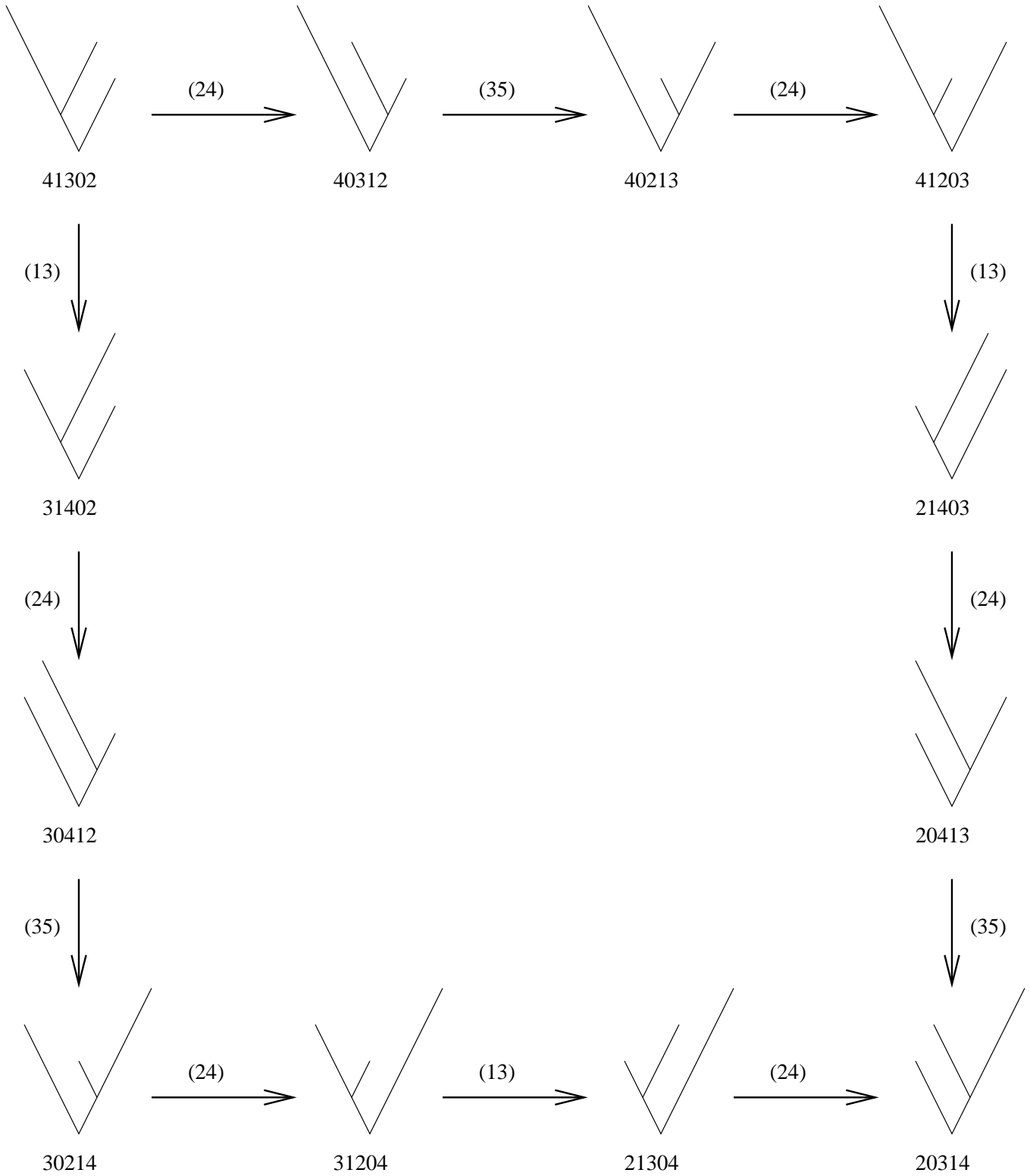




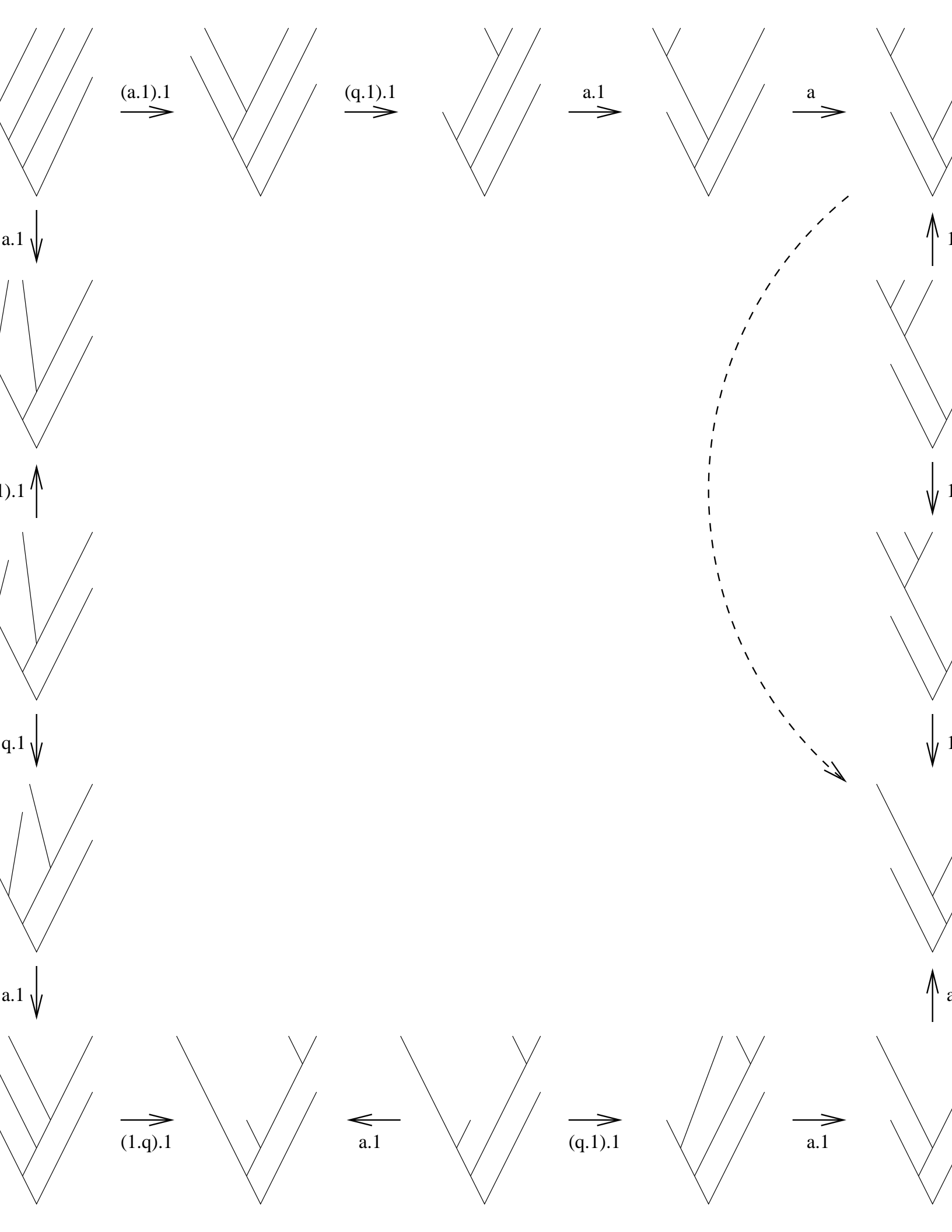


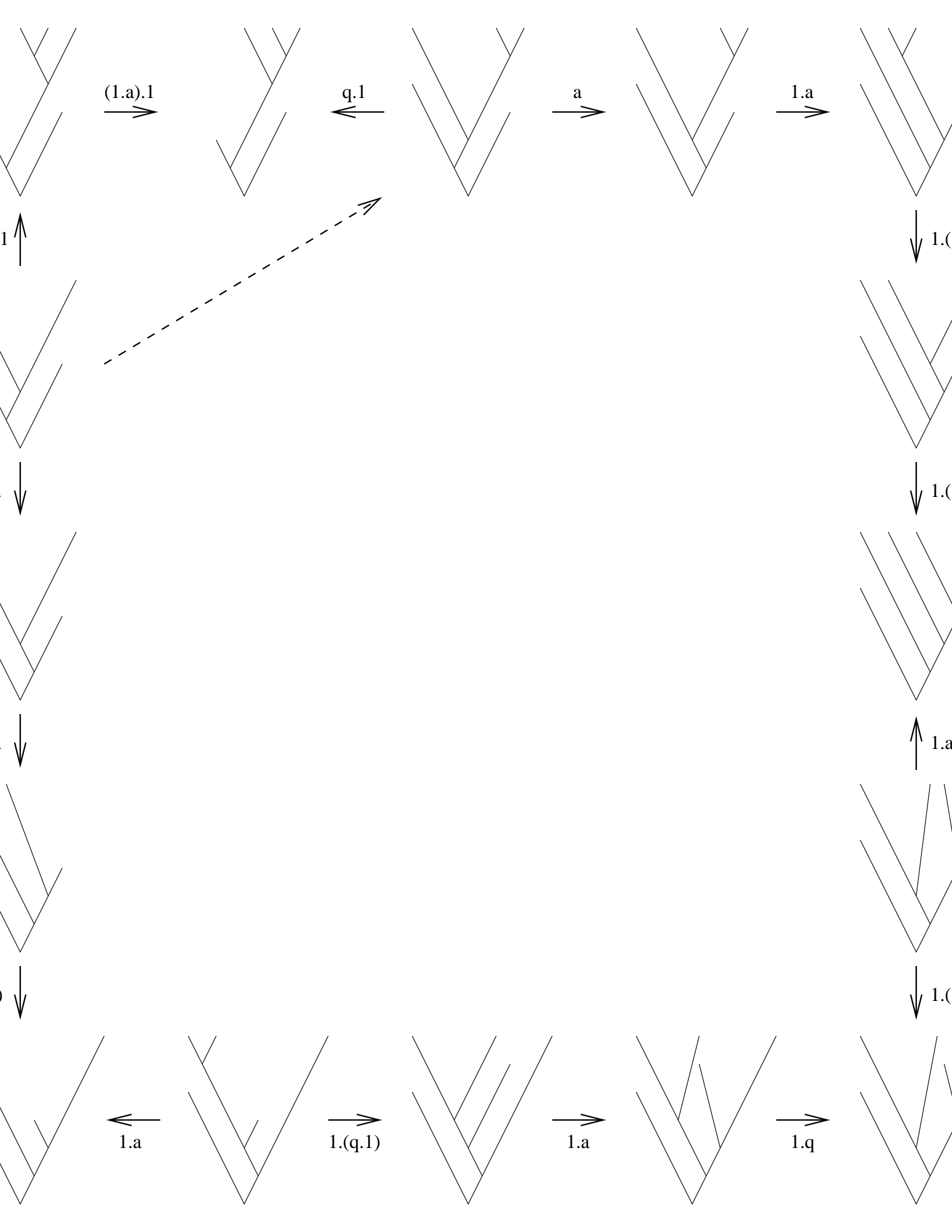


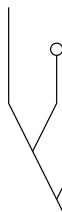
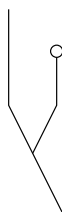
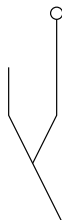


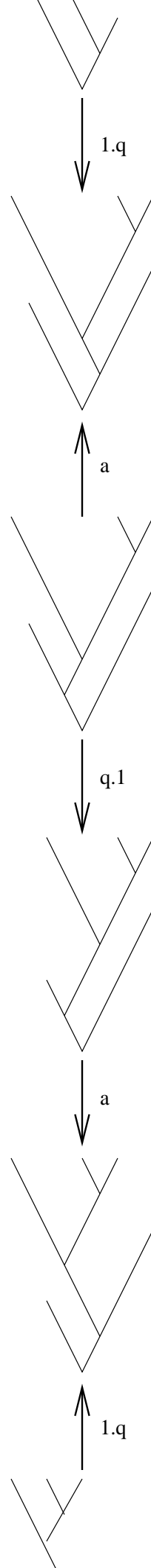
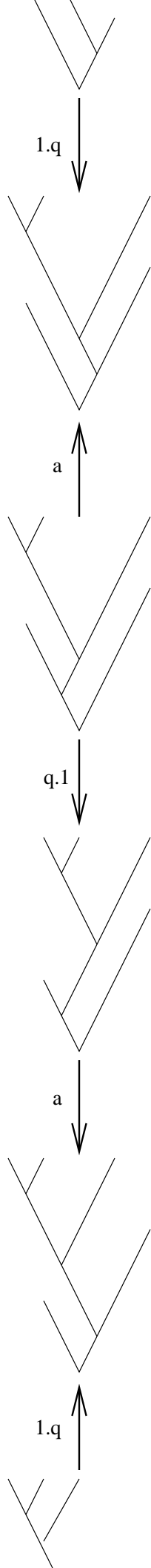












monoidal  
Bifunctor  
Natural isomorphism for associativity

Symmetric Premonoidal  
Natural isomorphism for commutativity  
c symmetric  
Hexagon diagram  
Square diagrams  
Decagon diagrams

q-Braided Premonoidal  
Natural isomorphism for interchange  
q-Pentagon diagram  
Dodecagon diagram

Symmetric q-Braided Premonoidal  
q symmetric

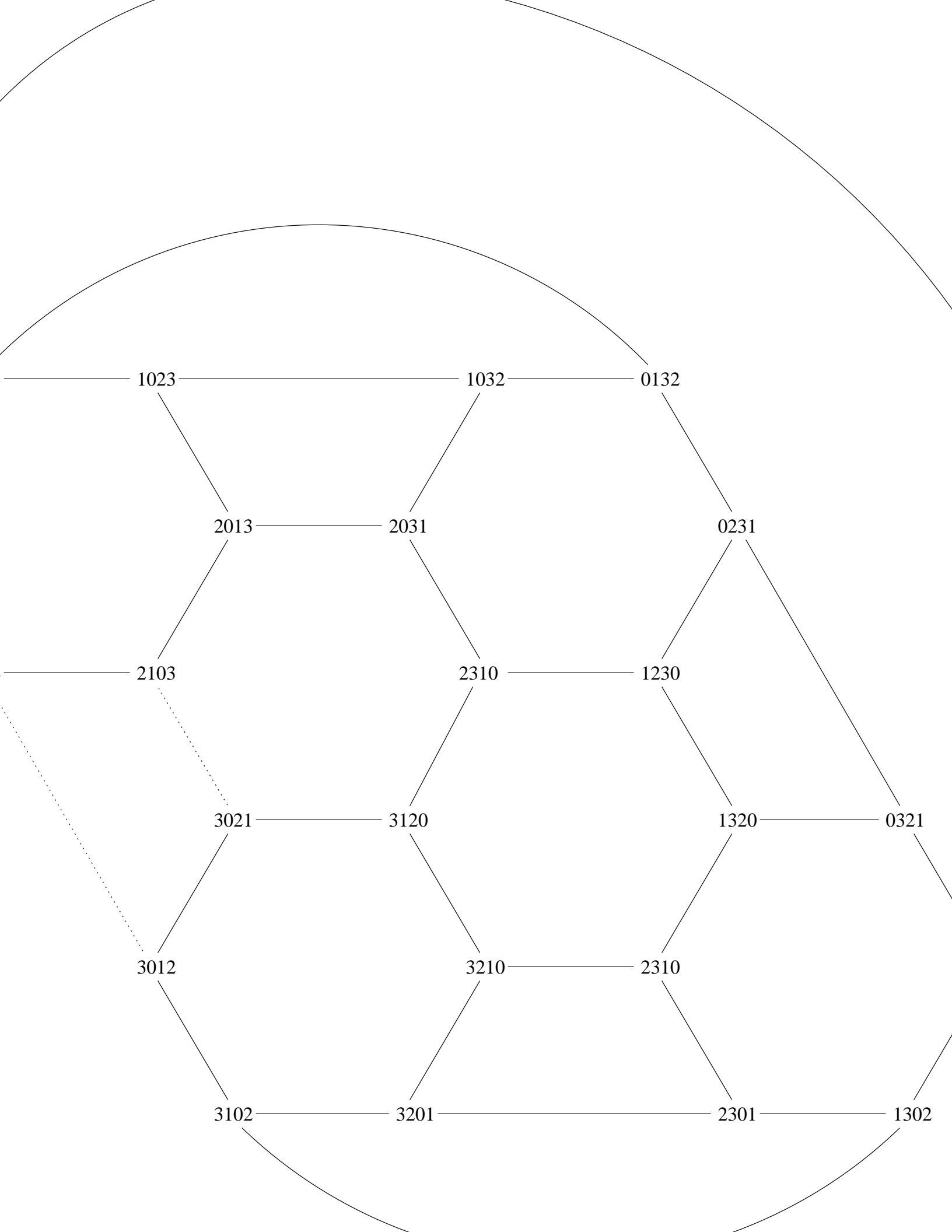
q-Premonoidal  
Quaddeacagon diagrams

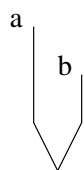
Symmetric q-Premonoidal

Monoidal  
Pentagon diagram  
Identity object  
Natural isomorphism for left and right identity  
Triangle diagram

Symmetric Monoidal

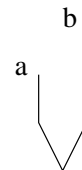
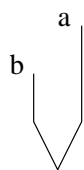
Symmetric q-Monoidal  
Identity object  
Natural isomorphism for left and right identity  
q-Triangle diagrams





$$q = \begin{array}{c} \text{U} \\ \text{S} \\ \text{U} \end{array}$$

The equation  $q =$  is followed by a diagram of a crossing. The strands are labeled 'a' and 'b' at the top and bottom. The crossing is a simple over-crossing.



$$q^{-1} = \begin{array}{c} \text{U} \\ \text{S} \\ \text{U} \end{array}$$

The equation  $q^{-1} =$  is followed by a diagram of a crossing. The strands are labeled 'a' and 'b' at the top and bottom. The crossing is a simple over-crossing.

